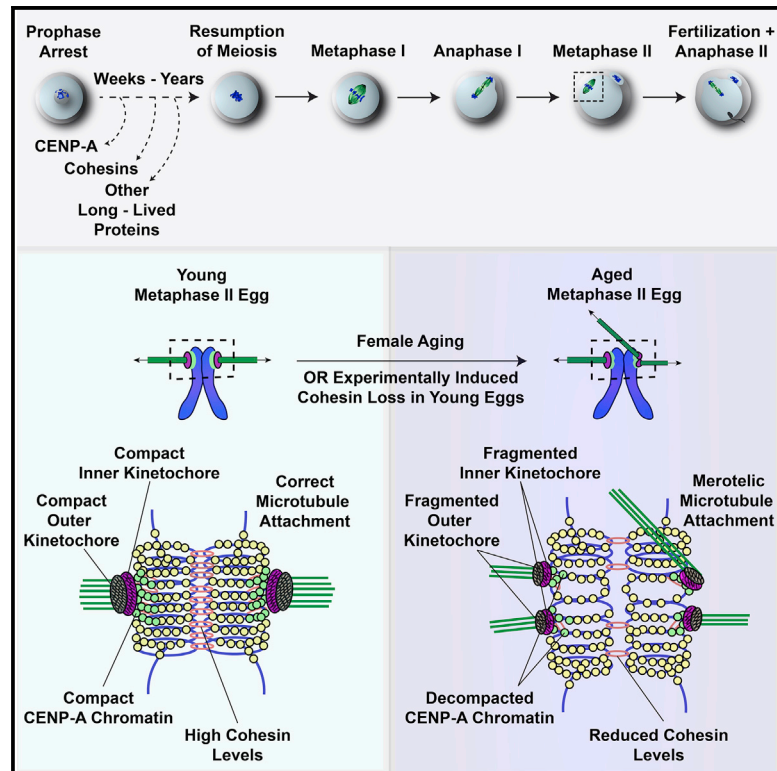**Article**

Meiotic Kinetochores Fragment into Multiple Lobes upon Cohesin Loss in Aging Eggs

Graphical Abstract

Authors

Agata P. Zielinska, Eirini Bellou,
Ninadini Sharma, ..., Kay Elder,
Eva R. Hoffmann, Melina Schuh

Correspondence

melina.schuh@mpibpc.mpg.de

In Brief

Aneuploidy in eggs increases dramatically as females age. Zielinska et al. show that aging affects the internal architecture of centromeres and kinetochores in mammalian eggs, including humans. As cohesin is lost, centromeric chromatin decompacts and kinetochores fragment, which is linked to incorrect chromosome-microtubule attachments.

Highlights

- Centromeric chromatin in oocytes decompacts as females age

- MI/MII kinetochores built on decompacted centromeres fragment into multiple lobes

- A partial loss of cohesin is sufficient to mimic these changes in young eggs

- Fragmented kinetochores frequently interact incorrectly with spindle microtubules

CellPress

CellPress

Meiotic Kinetochores Fragment into Multiple Lobes upon Cohesin Loss in Aging Eggs

Agata P. Zielinska,[1] Eirini Bellou,[1] Ninadini Sharma,[1] Ann-Sophie Frombach,[1] K. Bianka Seres,[1,2] Jennifer R. Gruhn,[3] Martyn Blayney,[2] Heike Eckel,[4] Rüdiger Moltrecht,[4] Kay Elder,[2] Eva R. Hoffmann,[3] and Melina Schuh[1,5,*]
[1]Max Planck Institute for Biophysical Chemistry, Am Fassberg 11, Göttingen 37077, Germany
[2]Bourn Hall Clinic, High Street, Cambridge CB23 2TN, UK
[3]DNRF Center for Chromosome Stability, Department of Cellular and Molecular Medicine, University of Copenhagen, Blegdamsvej 3, Copenhagen DK-2200, Denmark
[4]Kinderwunschzentrum, Kasseler Landstraße 25A, Göttingen 37081, Germany
[5]Lead Contact
*Correspondence: melina.schuh@mpibpc.mpg.de
https://doi.org/10.1016/j.cub.2019.09.006

SUMMARY

Chromosome segregation errors during female meiosis are a leading cause of pregnancy loss and human infertility. The segregation of chromosomes is driven by interactions between spindle microtubules and kinetochores. Kinetochores in mammalian oocytes are subjected to special challenges: they need to withstand microtubule pulling forces over multiple hours and are built on centromeric chromatin that in humans is decades old. In meiosis I, sister kinetochores are paired and oriented toward the same spindle pole. It is well established that they progressively separate from each other with advancing female age. However, whether aging also affects the internal architecture of centromeres and kinetochores is currently unclear. Here, we used super-resolution microscopy to study meiotic centromere and kinetochore organization in metaphase-II-arrested eggs from three mammalian species, including humans. We found that centromeric chromatin decompacts with advancing maternal age. Kinetochores built on decompacted centromeres frequently lost their integrity and fragmented into multiple lobes. Fragmentation extended across inner and outer kinetochore regions and affected over 30% of metaphase-II-arrested (MII) kinetochores in aged women and mice, making the lobular architecture a prominent feature of the female meiotic kinetochore. We demonstrate that a partial cohesin loss, as is known to occur in oocytes with advancing maternal age, is sufficient to trigger centromere decompaction and kinetochore fragmentation. Microtubule pulling forces further enhanced the fragmentation and shaped the arrangement of kinetochore lobes. Fragmented kinetochores were frequently abnormally attached to spindle microtubules, suggesting that kinetochore fragmentation could contribute to the maternal age effect in mammalian eggs.

INTRODUCTION

Chromosome segregation is driven by interactions between spindle microtubules and kinetochores, the macromolecular structures that assemble on centromeric nucleosomes containing the histone variant CENP-A [1–3]. These interactions allow the microtubule spindle to direct chromosome movement in space and time [4–6]. Failure to correctly attach all kinetochores generates cells with too many or too few chromosomes, a condition known as aneuploidy. Aneuploidy is particularly prominent in female meiosis: 20%–70% of human eggs carry an incorrect number of chromosomes, making chromosome segregation errors in oocytes a leading cause of pregnancy loss and human infertility [7–9].

Given the important role of kinetochores and centromeres in chromosome segregation, their structure has been studied extensively in mitosis [2, 10]. By contrast, our understanding of the internal architecture of centromeres and kinetochores in mammalian meiosis is still very limited. Studies in mice and humans have predominantly focused on the spacing between sister kinetochores during the two meiotic divisions [8, 9]. These studies revealed that the distance between sister kinetochores increases both in meiosis I [11–18] and meiosis II [17, 19–22] with advancing female age. This increase has been linked to an age-related loss of cohesin from chromosomes [23], as cohesins play an important role in sister kinetochore pairing and the cohesion between metaphase-I (MI) chromosomes and metaphase-II (MII) chromatids [11, 24–27]. In particular, centromeric cohesins pair sister kinetochores into a single functional unit during meiosis I, and physically link sister chromatids in meiosis II [28]. Cohesins are thought to be exceptionally long lived in oocytes and to gradually dissociate from chromosomes as females get older [12, 13, 23, 29, 30]. As cohesin levels decline, the space between sister kinetochores progressively increases. This has functional consequences for both meiosis I and meiosis II. Split meiosis-I sister kinetochores are more likely to form incorrect attachments to spindle microtubules [14, 17], and insufficient centromeric cohesion in meiosis II results in chromosomes separating prematurely into single chromatids [21, 31, 32] and aneuploidy [33–36]. However, although it is well established that sister kinetochores in oocytes separate
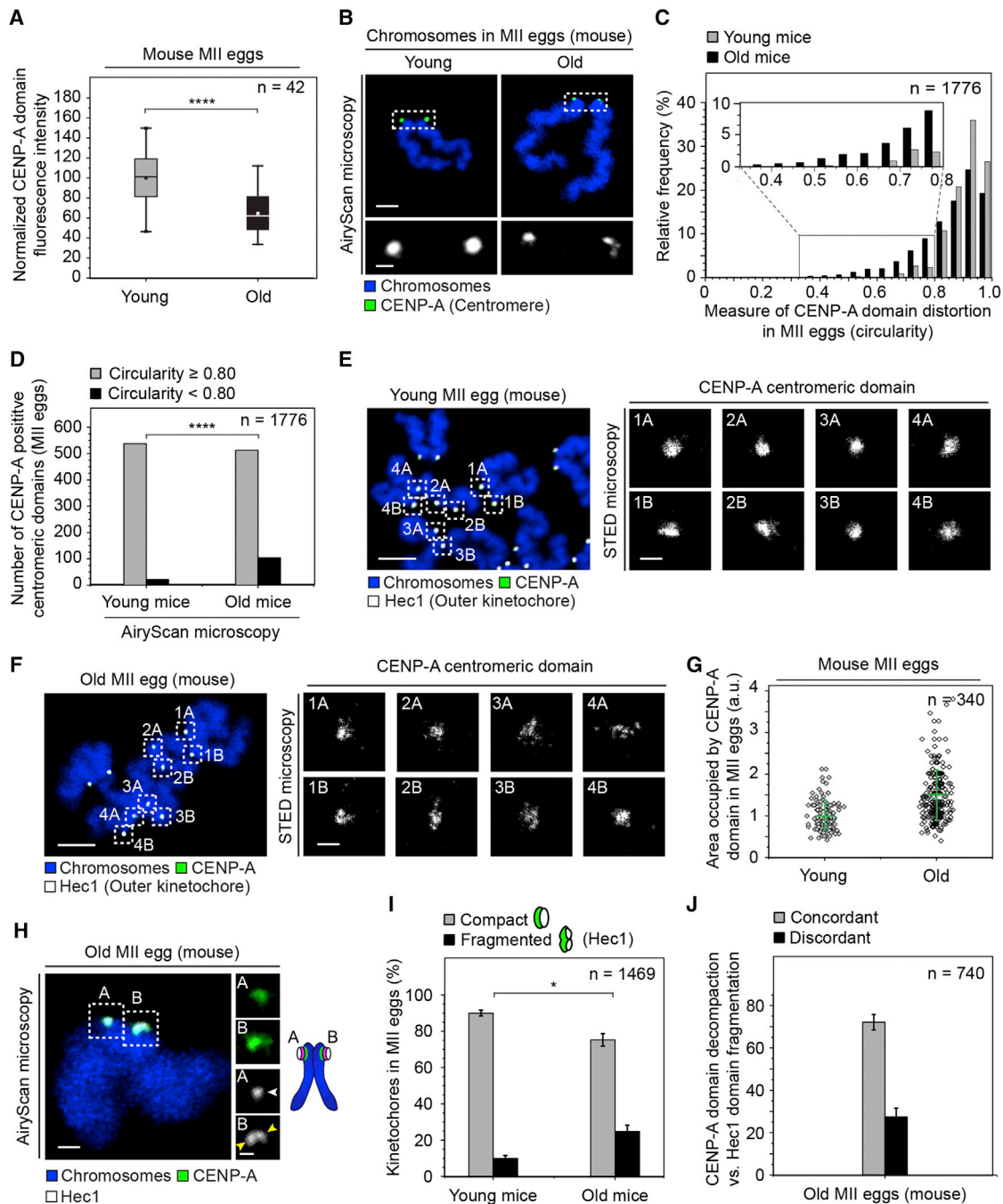
Figure 1. The Centromeric CENP-A Domain Decompacts as Oocytes Age and MII Kinetochores Built upon It Fragment into Lobes

(A) Centromeric CENP-A fluorescence intensity (integrated density of the centromeric region of interest [ROI] − mean background fluorescence × ROI) in 42 mouse MII eggs (3 independent experiments). 100% was assigned to the mean intensity of young groups. Box plots show median (horizontal white lines), mean (small white squares), 25th and 75th percentiles (boxes), and 5th and 95th percentiles (whiskers).

(B) Representative metaphase-II chromosomes from a young and an old mouse egg (8- and 62-week-old females, respectively) visualized with Airyscan microscopy (z projections of 14–16 sections, acquired every 0.18 μm). Centromeres (green, CENP-A) and DNA (blue, Hoechst) are shown. Scale bars represent 2 μm in overviews, and 0.5 μm in insets.

(C) Quantification of MII centromere circularity across the two age groups. A circularity value of 1.0 indicates a perfect circle. 1,776 measurements from 14 young and 17 aged MII eggs, imaged as in (B).

(D) Age-related increase in centromere distortion (circularity < 0.80) in MII eggs from young and old mice, imaged as in (B).

(E) Representative chromosome spread of a young MII mouse egg. DNA signal (blue, Picogreen, confocal mode), outer kinetochore region (white, Hec1, confocal mode), and the centromeric signal (green, CENP-A, STED mode) are shown. Right: one centromere in each panel (STED microscopy, grayscale; A and B, sister centromeres).

(legend continued on next page)

from each other as females age, we still know very little about the internal architecture of centromeres and kinetochores in aging mammalian oocytes.

Given the importance of the kinetochore in chromosome segregation, it is conceivable that changes in the internal architecture of centromeres and kinetochores could contribute to aneuploidy in aging oocytes. This seems plausible because oocyte kinetochores are built on a centromeric chromatin scaffold that can be several decades old at the time of chromosome segregation [37]. If and how centromeric chromatin changes with age, and whether this affects the architecture of the kinetochores that are built upon it, are currently unclear.

We therefore analyzed whether the internal organization of the meiotic centromere and kinetochore change as females age. In particular, we used quantitative super-resolution microscopy to analyze the architecture and function of 35,700 meiotic kinetochores in three mammalian species, including humans. In most experiments, we studied the internal architecture of kinetochores during metaphase of meiosis II, as sister kinetochores are spatially separated from each other during this stage, which greatly facilitates the analysis of individual kinetochores. By contrast, sister kinetochores are predominantly fused during metaphase I [38], which impedes the assessment of individual kinetochores and makes this stage less suitable for studies of internal kinetochore architecture.

Our analysis suggests that the centromeric CENP-A domain, on which the kinetochore is assembled, becomes decompacted with advancing female age. This was accompanied by fragmentation of inner and outer kinetochore regions into multiple lobes in over 30% of metaphase-II kinetochores of women and aged mice. An acutely induced loss of cohesin in eggs from young mice was sufficient to trigger the decompaction of CENP-A-containing chromatin, as well as kinetochore fragmentation, causing changes to the morphology of centromeres and kinetochores that closely resembled those in eggs from naturally aged females. Microtubule pulling further enhanced kinetochore fragmentation and shaped the pattern of the kinetochore lobules. Based on these data, we propose a model whereby the age-related cohesin loss not only favors aneuploidy by inducing a premature loss of cohesion within meiosis-I bivalents and meiosis-II chromosomes but also disrupts the organization of centromeric chromatin and thereby destabilizes the meiotic kinetochore in females.

RESULTS

The Centromeric CENP-A Domain Decompacts as Oocytes Age

To investigate whether aging affects the organization of centromeres, we used immunofluorescence microscopy to assess metaphase-II-arrested (MII) eggs from mice of different ages. In particular, we compared 8-week-old and 60- to 64-week-old FVB-N mice, which correspond to reproductively young and old females, as evident from a strong increase in aneuploidy in the aged group (Figure S1A).

MII centromeres in the aged group had strongly decreased levels of the centromere-specific histone variant CENP-A (Figure 1A), consistent with observations in prophase-arrested oocytes [39]. Strikingly, the centromeres also differed in their architecture. Whereas young centromeres had a compact CENP-A signal when visualized with Airyscan microscopy (Figure 1B, left panel), aged centromeres were often organized into multiple CENP-A subunits (Figure 1B, right panel) and frequently appeared decompacted (Figures 1C and 1D).

Stimulated emission depletion (STED) microscopy, which has greater resolving power [40], revealed multiple clustered CENP-A foci within the aged centromeric domain (Figures 1F and S1B). This was in contrast to the compact appearance of centromeres in young eggs (Figures 1E and S1B). Consistent with age-related decompaction, the CENP-A domain was distributed over a larger surface area in eggs from older mice (Figure 1G). Decompaction of individual centromeres into multiple subunits was also evident in meiosis-I bivalents (Figure S1C, yellow arrowheads), suggesting that it is a general feature of aged meiotic centromeres. Altogether, these results establish that centromeric chromatin in oocytes and eggs decompacts as females age.

Kinetochores Built on Decompacted Centromeres Fragment into Lobes

Next, we asked whether kinetochores, which assemble upon centromeres, also show age-related changes in mammalian eggs. We first examined the outer kinetochore components on chromosome spreads. The outer kinetochore Hec1 domain that directly interacts with spindle microtubules appeared distorted in aged mouse eggs, and was frequently fragmented into two prominent lobes (Figures 1H, 1I, and S1D). In 75% of cases, the centromeric CENP-A region and the Hec1 kinetochore domain were concordant, with both appearing either

---

(F) Representative chromosome spread of an MII egg from an old mouse (63 weeks), labeled as in (E).
(G) Surface area of CENP-A centromeric domains in MII eggs from young and aged mice, acquired as in (E) and (F). Distortion of the centromeric domain was measured as the surface area of the smallest circle encompassing the CENP-A signal (119 young and 221 aged centromeres analyzed). Mean and SD are shown.
(H) Representative Airyscan-imaged metaphase-II chromosome from an aged mouse egg (61-week-old female). Outer kinetochores (white, Hec1), centromeres (green, CENP-A), and DNA (blue, Hoechst) are shown. Scale bars represent 1 μm in overview, and 0.5 μm in insets.
(I) Quantification of kinetochore configurations visualized with Airyscan microscopy, based on the outer Hec1 signal in 37 MII mouse eggs (3 experiments), labeled as in (H).
(J) Quantification of how frequently the MII outer kinetochore pattern follows changes in the underlying centromeric domain. Concordant indicates centromere/outer kinetochore pairs where the CENP-A/Hec1 signals were both either compact or fragmented. 740 centromeres and their corresponding kinetochores from 19 old MII mouse eggs (3 experiments), labeled as in (B) and (H).
Young MII eggs: 8-week-old females; aged eggs (12 animals): 60- to 64-week-old females. Scale bars represent 4 μm in overviews, and 0.5 μm in insets in (E) and (F). p values are designated as *p < 0.05 and ****p < 0.0001. p values were calculated with Student's t test (I) and Fisher's exact test (D). In (A), mean fluorescence measurements per egg were compared by one-way ANOVA followed by Tukey's test. Error bars show SEM. White arrows point to compact kinetochores, and yellow arrows point to lobes within a fragmented MII kinetochore.
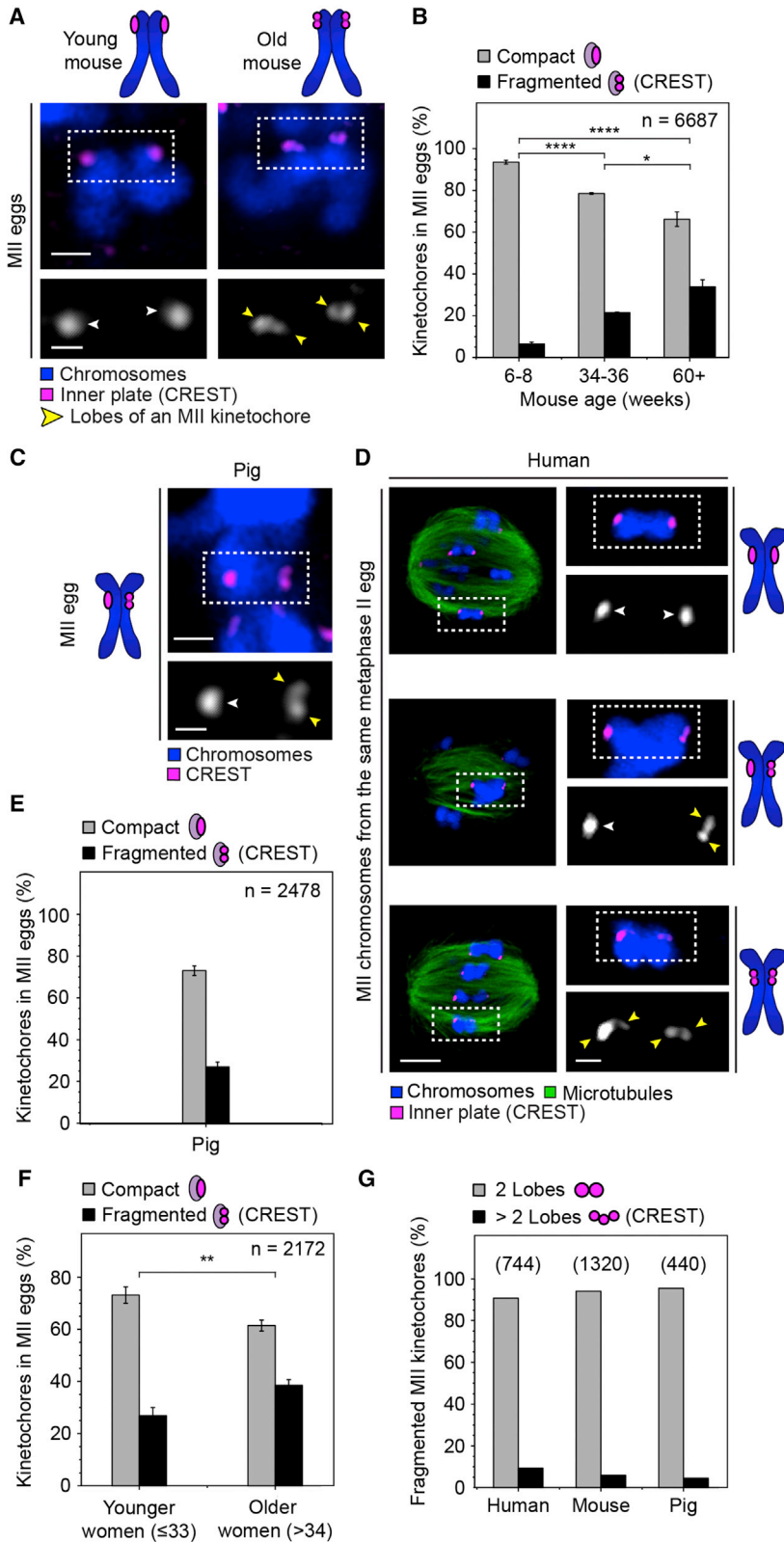See also Figure S1.

Figure 2. Kinetochore Fragmentation Is Conserved across Various Mammalian Species

(A) Examples of kinetochores in MII eggs from young (8 week) and aged (≥60 week) mice.

(B) Kinetochore configurations shown in (A) and their occurrence in 176 MII eggs from mice of different ages (6 experiments; aged eggs originated from 29 mice).

(C) Representative pig metaphase-MII chromosome and its corresponding kinetochores.

(D) Three representative human MII chromosomes from the same egg (33-year-old donor). Scale bars represent 4 μm in overview, and 0.5 μm in insets.

(E) Kinetochore configurations shown in (C) and their occurrence in 63 pig MII eggs (8 experiments).

(F) Kinetochore configurations shown in (D) and their occurrence in 17 MII eggs from young (≤33 years old) and 32 MII eggs from older (>34 years old) women.

(G) Multi-lobular kinetochore configurations (2 or >2 distinct lobes) and their occurrence in MII eggs from humans, pigs, and aged mice.

Kinetochores (magenta, CREST) and DNA (blue, Hoechst) are shown in (A), (C), and (D). In (D), microtubules are additionally labeled (green, α-tubulin). Chromosomes were fixed on intact spindles at the metaphase-II stage and imaged with Airyscan microscopy.

Scale bars represent 1 μm in overview, and 0.5 μm in insets in (A) and (C)

p values are designated as *p < 0.05, **p < 0.01, and ****p < 0.0001. All p values were calculated with Student's t test. Error bars show SEM. White arrows point to compact kinetochores, and yellow arrows point to lobes within a fragmented MII kinetochore.
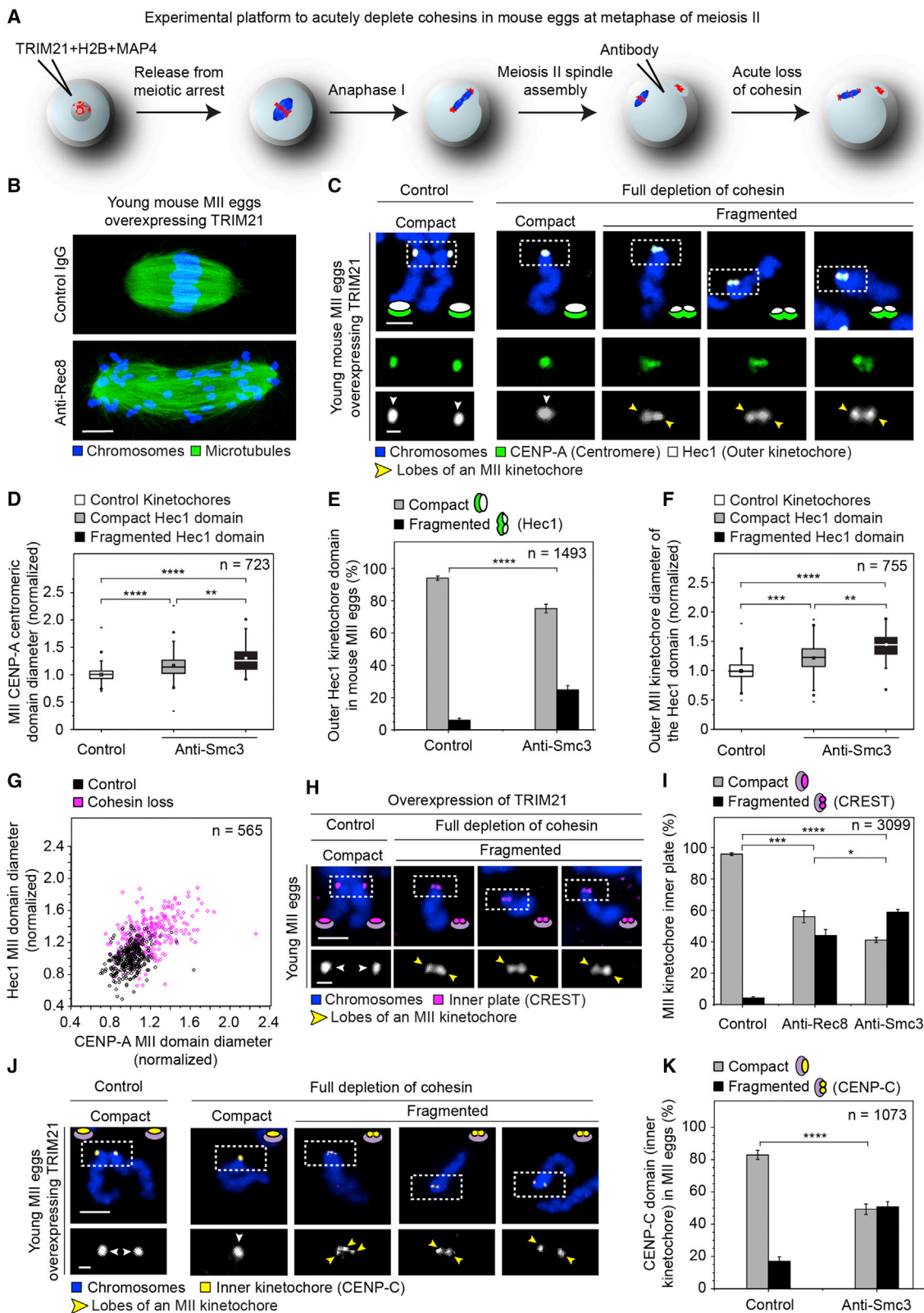
See also Figure S2.

Figure 3. Cohesin Loss Causes Decompaction of Centromeric Chromatin and Fragmentation of Meiotic Kinetochores

(A) Scheme of Trim-Away experiments to acutely degrade cohesins in mouse metaphase-II eggs. Trim-Away is a protein depletion tool, which uses antibodies to rapidly remove unmodified, native proteins via the antibody receptor/E3 ubiquitin ligase TRIM21 and the endogenous protein degradation machinery.

(legend continued on next page)

compact or fragmented (Figure 1J). Centromere decompaction hence correlates with the fragmentation of the outer kinetochore domain, and both are increased in aged mouse eggs.

We then tested whether the age-related changes in centromere and kinetochore architecture are also evident in intact eggs, in which the three-dimensional arrangement of chromosomes on the spindle is preserved. Because the majority of super-resolution techniques are not compatible with the size of mammalian oocytes, we employed Airyscan microscopy to establish whether the bilobed appearance is evident across the kinetochore complex. We labeled inner kinetochore plates (Figure S2A) with CREST antisera (Figure 2A), which mark predominantly CENP-B [41]. Consistent with the observations for Hec1, CREST-labeled inner kinetochore plates appeared as fragmented foci in 6% and 21% of MII eggs from mice aged 8 weeks and 34–36 weeks, respectively (Figure 2B, left and middle panels). The frequency of kinetochore fragmentation further increased to over 33% in eggs from mice older than 60 weeks (Figure 2B, right panel). The changes in MII kinetochore architecture between young and aged eggs could not be attributed to differences in the time required for the oocytes to progress through meiosis I (Figure S2B). They were also not an artifact of the imaging conditions that we used, because mitotic kinetochores under identical conditions appeared as single compact structures (Figures S2C and S2D). Together, these data suggest that inner and outer kinetochore regions fragment into lobes in aged mouse eggs.

Kinetochore Fragmentation Is Conserved across Various Mammalian Species
To establish whether fragmented kinetochores are also present in other species, we examined eggs from humans and pigs (Figures 2C and 2D). Around 25% of kinetochores were fragmented in MII eggs from pre-pubertal pigs and young women (Figures 2E, 2F, and S2E–S2H). The kinetochore inner plates here also predominantly reorganized into two lobes (Figure 2G). Consistent with our findings in aged mice, kinetochore fragmentation in human MII eggs became more apparent with advancing age, affecting 39% of meiotic kinetochores in women over 34 years (Figure 2F). Furthermore, in human kinetochores that appeared bilobular, the fragmentation similarly affected multiple layers of the kinetochore complex, as evident from the bilobular appearance of outer plates marked with Hec1 and CENP-F and the fibrous corona labeled with BubR1 (Figure S2I). Together, these data suggest that fragmentation is a prominent and widely conserved feature of the meiotic kinetochore that is already present in young women but becomes more pronounced with advancing age.

Cohesin Loss Causes Decompaction of Centromeric Chromatin and Fragmentation of Meiotic Kinetochores
We next investigated the mechanism underlying the age-related decompaction of centromeric chromatin and kinetochore fragmentation. We wondered whether the architectural changes that we observed might be linked to the loss of cohesin from chromosomes, which is well established to occur with advancing maternal age [12, 13, 30, 42]. Cohesin might be required to arrange CENP-A-containing chromatin into a compact platform that is suitable for the assembly of stable kinetochores in mammalian oocytes. This model predicts that a loss of cohesin would be sufficient to trigger CENP-A domain decompaction and kinetochore fragmentation.

To test this hypothesis, we used the Trim-Away approach to remove cohesin acutely in metaphase of meiosis II (Figure 3A). Trim-Away utilizes antibodies to target unmodified, native

(B) Immunolabeled young TRIM21 overexpressing metaphase-II mouse eggs, microinjected with either a control IgG antibody (top) or an anti-Rec8 antibody provided in excess (bottom), as in (A). Images are z projections of 63–69 sections, acquired every 0.19 μm. Microtubules (green, α-tubulin) and chromosomes (blue, Hoechst). The scale bar represents 5 μm.

(C) Representative chromosome spreads from young metaphase-II mouse eggs depleted of Smc3. Insets: a chromosome (control, left panel) or individual single chromatids (all other panels). Outer kinetochores (white, Hec1), centromeres (green, CENP-A), and chromosomes (blue, Hoechst) are shown.

(D) Normalized diameter of the CENP-A centromeric domain in control and young mouse MII eggs depleted for Smc3, as in (C). CENP-A domains were divided into three groups, based on the fragmentation status of the overlying Hec1 kinetochore. 723 centromeres from 20 MII eggs were evaluated (2 experiments).

(E) Occurrence of different kinetochore architectures based on outer kinetochore Hec1 signal in cells treated as in (C). Data are from 35 MII eggs (young mice; 2 experiments).

(F) Normalized diameter of the Hec1 kinetochore domain in control and young mouse eggs depleted for Smc3. Both the fragmentation status and the diameter measurements were based on Hec1 labeling. 755 kinetochores from 20 MII eggs were evaluated (2 experiments).

(G) The diameter of the CENP-A centromeric domain (a.u.) plotted against the Hec1 outer kinetochore domain diameter (a.u.) for each of the 565 MII kinetochores following a full depletion of Smc3/control MII eggs as in (C). Pearson's correlation coefficients: $r = 0.402$ (controls) and $r = 0.495$ (experimental group).

(H) Inner plates of MII kinetochores in metaphase-arrested eggs from young mice in a control chromosome (left panel; two sister kinetochores) and in single chromatids induced by a full depletion of Rec8 (other panels), achieved as in (B). Chromosomes (blue, Hoechst) and kinetochore inner plates (magenta, CREST) are shown.

(I) Occurrence of MII kinetochore configurations in young eggs following the targeting of distinct cohesin subunits (Rec8, Smc3) by Trim-Away (full depletion) and in control eggs. Data are from 79 MII eggs from young mice (3 experiments).

(J) Young metaphase-II eggs labeled with the inner kinetochore protein CENP-C. Images show a control chromosome (left panel; two sister kinetochores) and single chromatids induced by a full depletion of Rec8 (other panels), obtained as in (A). Chromosomes (blue, Hoechst) and kinetochore inner plates (yellow, CENP-C) are shown.

(K) Occurrence of different kinetochore architectures based on the inner kinetochore CENP-C signal in cells treated as in (J). Data from 36 MII eggs (young mice; 2 experiments).

Scale bars represent 2 μm in overviews, and 0.5 μm in insets in (C), (H), and (J).

p values are designated as $*p < 0.05$, $**p < 0.01$, $***p < 0.001$, and $****p < 0.0001$. p values were calculated with Student's t test in (I) and Fisher's exact test in (E) and (K); in (D) and (F), mean measurements per egg were compared by one-way ANOVA followed by Tukey's test. Error bars show SEM. Box plots show median (horizontal lines), mean (small squares), 25th and 75th percentiles (boxes), and 5th and 95th percentiles (whiskers). Arrows: white point to compact kinetochores, and yellow point to lobes within a fragmented MII kinetochore.
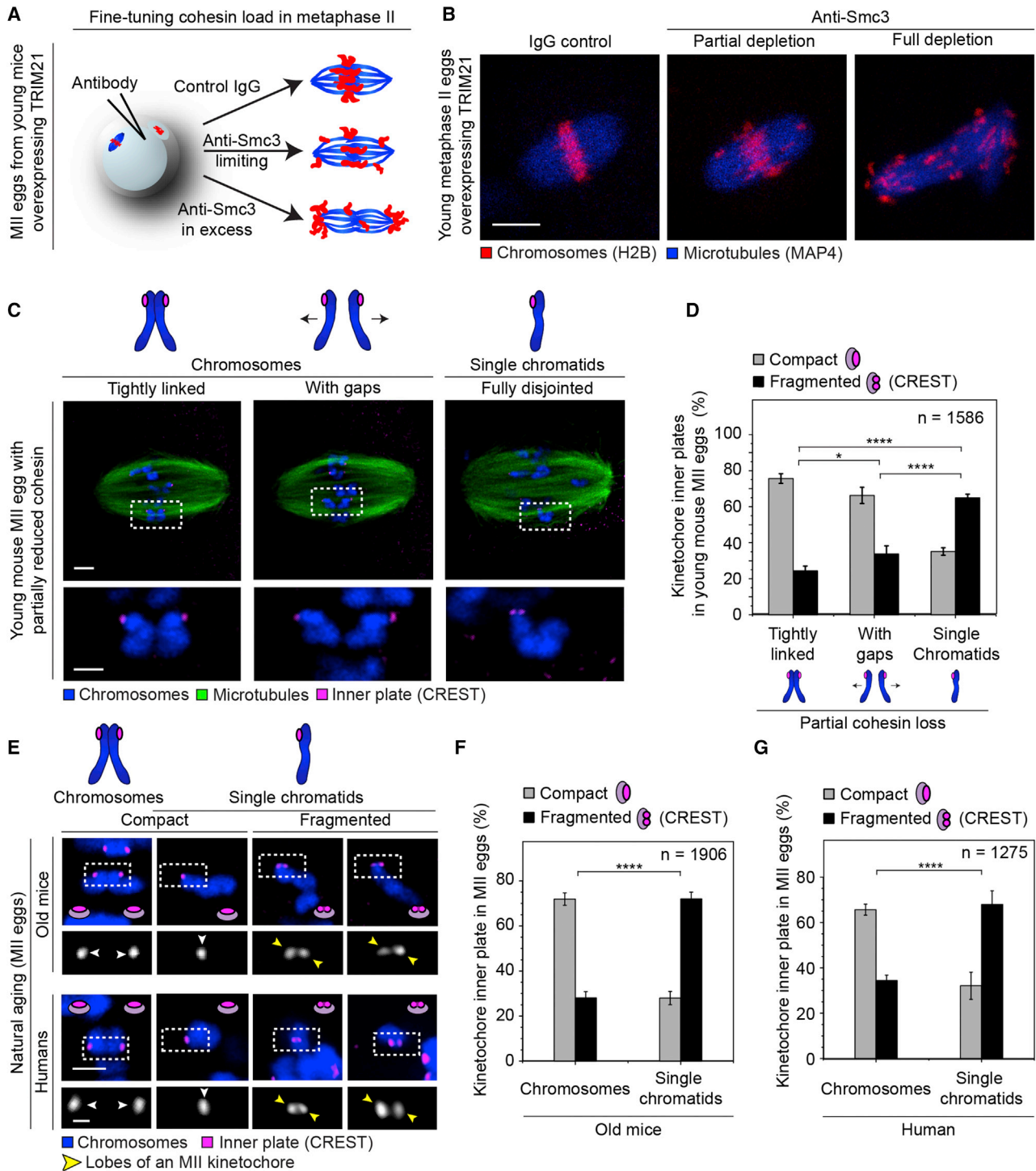
See also Figures S3–S5 and Videos S1 and S2.

Figure 4. The Extent of Kinetochore Fragmentation Correlates with the Degree of Cohesion Loss

(A) Scheme of the partial Trim-Away method in metaphase-II eggs. The degree of cohesin loss is fine-tuned by varying the amount of microinjected antibody.

(B) Representative live spindles from TRIM21-overexpressing young MII eggs microinjected with either a control IgG antibody or various concentrations of the anti-Smc3 antibody. Chromosomes (red, H2B-mRFP) and microtubules (blue, MAP4-MTBD-Snap647). The scale bar represents 10 μm.

(C) Representative examples of the three chromosome categories aligned at the equator of the same metaphase-II spindle following partial depletion of Smc3 by Trim-Away, as in Figure S5E.

(D) Occurrence of different MII kinetochore architectures based on CREST signal in the three chromosome categories defined by Hoechst signal, as in (C), following partial depletion of Smc3 (41 young MII eggs, 4 experiments).

(legend continued on next page)

proteins for proteasome-mediated degradation via the antibody receptor/E3 ubiquitin ligase TRIM21 [43]. In particular, we used two independent approaches to target the meiotic cohesin complex in eggs, using antibodies against the cohesin subunit Smc3 [44] and the meiosis-specific α-kleisin variant Rec8 [24, 45–47]. Quantitative immunofluorescence of Rec8 (Figures S3A–S3C) and Smc3 (Figures S3D and S3E) on chromosome spreads confirmed that Trim-Away of either subunit resulted in removal of cohesin complexes from the centromeric regions of MII chromosomes. Consistent with centromeric cohesin removal, all chromosomes separated into single chromatids within minutes of Rec8 or Smc3 antibody microinjection (Figures 3B, S3F, and S3G; Video S1). Thus, Trim-Away with antibodies against either Rec8 or Smc3 is consistent, and efficiently depletes centromeric cohesins in metaphase-II-arrested eggs from young mice.

We then assessed whether acute removal of cohesin was sufficient to reproduce the changes in centromeric chromatin and kinetochore architecture that we had observed in aged mice. Indeed, degradation of Smc3 caused a prominent decompaction of centromeric chromatin (Figures 3C, 3D, and S4A) and fragmentation of the Hec1 domain into two lobes (Figures 3C, 3E, 3F, S4B, and S4C). Importantly, the increased diameter of the Hec1 domain positively correlated with the size of the underlying CENP-A centromeric domain (Figure 3G), further supporting our model that the age-related changes in centromere and kinetochore architecture are coupled. Moreover, the inner kinetochore plates (marked by CREST and CENP-C; Figures 3H–3K, S4D, and S5A; Video S2), as well as the fibrous corona (marked by BubR1; Figures S5B and S5C), also frequently fragmented into two lobes upon cohesin removal. Together, these data establish that a loss of cohesin is sufficient to trigger the decompaction of centromeric chromatin and the fragmentation of inner and outer kinetochore regions, closely resembling the changes in centromere and kinetochore architecture that we observed in aged eggs.

The Extent of Kinetochore Fragmentation Correlates with the Degree of Cohesion Loss

Chromosomes in aged MII eggs are affected by loss of cohesin to different degrees [31]. Metaphase-II chromosomes in which cohesin is depleted to a lesser degree remain intact, with both chromatids still linked, and only the distance between their sister kinetochores increases. By contrast, chromosomes with more severe cohesin depletion separate completely into single chromatids (Figure S5D). To reproduce these different chromosome architectures in eggs from young females, we modified the Trim-Away approach to enable a partial depletion of cohesin by using lower amounts of the Smc3 antibody (Figures 4A and S5E–S5G). Under these conditions, only a subset of metaphase-II chromosomes separated into single chromatids (Figure 4B, middle

panel and Figure S5E), although the proportion of disjointed chromosomes was still higher than following natural aging (Figure S5D). We then used young mouse eggs partially depleted of cohesins, as well as eggs from aged mice, to determine whether the extent of cohesion loss correlates with the extent of kinetochore fragmentation.

In young eggs with partially reduced cohesin, 67% of CREST-labeled kinetochores on single chromatids were fragmented, in comparison to only 28% on intact chromosomes (Figures 4C and 4D, left and right panels). Also within the intact chromosome class, the degree of cohesion between sister chromatids differed: some sister chromatids remained tightly associated, indicative of high cohesion levels, whereas others were still connected but separated by prominent gaps, indicative of reduced cohesion (Figure 4C, "tightly linked" and "with gaps"). Interestingly, closely associated chromatids (Figure 4D, left panel) were less likely to show kinetochore fragmentation than chromatids with gaps (Figure 4D, middle panel). This correlation between kinetochore fragmentation and the degree of cohesion loss was also apparent in naturally aged MII eggs from mice and humans (Figures 4E–4G; Video S3). Together, these data establish that the degree of cohesion loss correlates with the degree of kinetochore fragmentation.

Kinetochore Fragmentation Is Also Evident during Meiosis I

Our data established that MII kinetochores frequently fragment into multiple lobes in eggs of various mammalian species (Figure 2). However, the oocyte segregates its chromosomes twice. Because cohesion in aged oocytes is already reduced in meiosis I [8, 23], kinetochore fragmentation could in principle affect both divisions of the mammalian oocyte.

In line with this idea, fragmented kinetochores could also be detected in meiosis I in both naturally aged human and mouse oocytes (Figures S6A and S6B). To establish whether cohesin loss is also sufficient to trigger kinetochore fragmentation during meiosis I, we modified our Trim-Away approach to partially deplete cohesins at metaphase I (Figure 5A). In particular, we determined conditions that maintained homologous chromosome pairing in mouse oocytes (Figures 5B, 5C, and S6C) but caused an increase in sister kinetochore distance to a degree that we have previously reported in naturally aged human oocytes from women in their mid-thirties (Figure 5D) [17], indicative of reduced cohesion in the centromeric region.

The separation of sister kinetochores upon partial cohesin depletion (Figures 5D and 5E) was indeed coupled to changes in kinetochore architecture (Figures 5E–5G, S6D, and S6E). Despite the high proximity of sister kinetochores in meiosis I, a significant fraction of MI kinetochores became visibly

(E) Representative kinetochores in chromosomes (left panels) and single chromatids (all other panels) in MII eggs from aged mice (≥60 weeks) or women of all ages.
(F) Kinetochore architectures shown in (E) and their occurrence on intact chromosomes and single chromatids (50 metaphase-II eggs from aged mice, 5 experiments).
(G) Kinetochore architectures shown in (E) and their occurrence on intact chromosomes and single chromatids in 29 human MII eggs.
Scale bars, 2 μm in overview, and 0.5 μm in insets. Chromosomes (blue, Hoechst) and kinetochores (magenta, CREST) are shown in (C) and (E). In (C), microtubules are additionally labeled (green, α-tubulin).
p values are designated as *p < 0.05 and ****p < 0.0001. p values were calculated with Fisher's exact test. Error bars show SEM. Arrows: white point to compact kinetochores, and yellow point to lobes within a fragmented MII kinetochore.
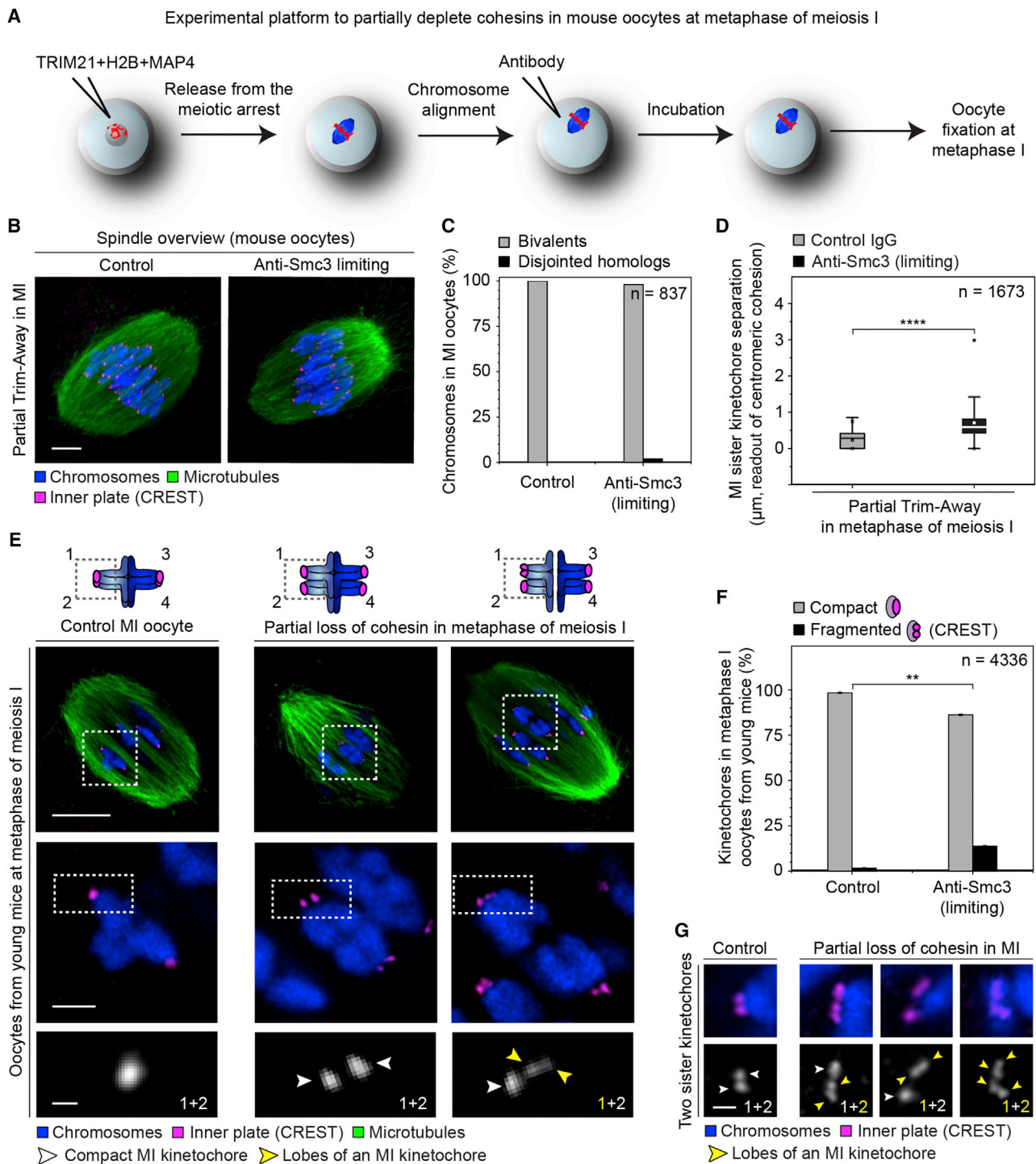See also Figure S5 and Video S3.

Figure 5. Kinetochore Fragmentation Is Also Evident during Meiosis I

(A) Scheme of the partial Trim-Away method in metaphase I, where cohesin levels are reduced by microinjecting an anti-Smc3 antibody at a limiting concentration.

(B) Representative Trim-Away spindles at late metaphase I, in young mouse oocytes microinjected with a control antibody (left panel) or with an anti-Smc3 antibody at a limiting concentration (right panel). Images are z projections of 82 sections acquired every 0.18 μm. The scale bar represents 5 μm.

(C) Occurrence of different chromosome architectures assessed based on the Hoechst signal in MI oocytes treated as in (B). Data are from 42 young MI oocytes (2 experiments).

(D) Distance between the two sister kinetochores of a bivalent in metaphase-I oocytes from young mice treated as in (B). Data are from 42 young MI oocytes (2 experiments). Box plots show median (horizontal white lines), mean (small white squares), 25th and 75th percentiles (boxes), and 5th and 95th percentiles (whiskers).

(legend continued on next page)

fragmented (Figures 5F, 5G, and S6E). Thus, as cohesins are lost, sister kinetochores not only uncouple but individual MI kinetochores also fragment into lobes.

Fragmented Kinetochores Are More Likely to Be Abnormally Attached to Spindle Microtubules

Next, we investigated how fragmented kinetochores interact with microtubules. We first examined whether fragmented kinetochores are still able to attach to the spindle. To achieve this, we selectively visualized kinetochore-bound microtubules (called k-fibers) by briefly exposing mouse eggs to cold [48]. This revealed that fragmented kinetochores are predominantly still functional: the number of unattached kinetochores in intact chromosomes did not differ significantly between the compact and fragmented kinetochore groups (Figure S7A). However, whereas over 90% of intact kinetochores attached as expected to one k-fiber only, 49% of fragmented kinetochores were attached to two distinct k-fiber bundles (Figure 6A).

Because kinetochores become compartmentalized into two lobes with age and each fragment frequently interacts with an independent k-fiber bundle, we wondered whether fragmented kinetochores are also more likely to be merotelically attached (Figure 6B). Chromosome segregation errors often result from merotelic attachments, where a single kinetochore is simultaneously bound to microtubules from opposite spindle poles [14, 49–51]. These merotelically attached kinetochores will lag at anaphase onset, increasing the chances of mis-segregation [49]. Our analysis revealed that over 31% of fragmented kinetochores were merotelically attached, compared to only 7% of intact kinetochores (Figure 6C). Frequently, only one fragment interacted with each spindle pole ("bilobular merotelic," Figures 6D and 6E). This observation may also explain why single chromatids were often able to align in the center of the meiotic spindle (Figures 6D and S7B) [50], despite having a single kinetochore only. Although chromosome alignment is generally thought to rely on two distinct kinetochores that attach to spindle microtubules originating from opposite spindle poles, these data suggest that single meiotic kinetochores can also promote alignment of single chromatids, by splitting into two lobes, which both attach to k-fibers from opposite spindle poles (Figure 6D). Together, these data establish that kinetochore fragmentation correlates with abnormal kinetochore-microtubule attachments.

Microtubule Pulling Enhances and Shapes Kinetochore Fragmentation

Why are kinetochore fragmentation and merotelic attachments correlated? The age-related decompaction of centromeric chromatin and its associated kinetochore could broaden and distort the microtubule-interacting surface, which could hinder the establishment of correct microtubule attachments. Kinetochores with lateral or end-on merotelic attachments would experience pulling from opposite directions, which could further enhance their fragmentation. Centromeric chromatin decompaction and microtubule pulling could thereby generate a positive feedback loop, which would manifest in merotelic attachments and prime eggs for chromosome segregation errors. The strain on meiotic kinetochores could be further enhanced by the dynamics of spindle assembly in meiosis: kinetochores in oocytes are exposed to prolonged pulling, because meiotic spindles in both female mice and women take multiple hours to assemble fully [52–55], in a process which in humans involves several hours of spindle reorganization [54].

To test directly whether microtubule pulling enhances kinetochore fragmentation, we decreased microtubule-dependent pulling by treating eggs with the microtubule-depolymerizing drug nocodazole. We opted for a concentration of the drug at which the pulling experienced by kinetochores is reduced but the general bipolar organization of the spindle is maintained and thus chromosomes are sufficiently individualized for kinetochore analysis. We then induced kinetochore fragmentation by Trim-Away of Smc3. We found that kinetochore fragmentation was reduced from 52% in DMSO-treated control eggs to 35% in eggs treated with low doses of nocodazole (Figure 6F). This suggests that microtubule pulling enhances fragmentation.

Our analysis also revealed that meiotic kinetochores preferentially reorganize their fragments into two distinct lobes (Figure 2G). We wondered whether the bilobular appearance of the fragmented meiotic kinetochore reflects an inherent structural feature of kinetochores in meiosis, or whether it could result from clustering of multiple kinetochore fragments into two large groups by bidirectional pulling from the two spindle poles. To discriminate between these possibilities, we treated control and partially Smc3-depleted oocytes from young mice with monastrol at the onset of meiosis I, to completely eliminate the exposure of meiotic kinetochores to bidirectional pulling (Figure S7C). Monastrol treatment leads to the formation of a microtubule ball that contains multiple microtubule-organizing centers (MTOCs) and carries the chromosomes on its surface [56, 57]. Kinetochores were still fragmented in monastrol-treated oocytes (Figures 6G and 6H, monastrol groups). However, instead of always forming two domains, some kinetochores fragmented into multiple lobes (Figures 6G and S7D). Interestingly, monastrol treatment enhanced kinetochore fragmentation even in young control mouse oocytes, without depletion of cohesin (Figure 6G, right top panel; and Figure 6H, second column). This might be due to altered pulling forces exerted on kinetochores by the

(E) Representative Trim-Away spindles treated as in (B). Insets: chromosome and kinetochore architectures in MI bivalents under these conditions. Scale bars represent 10 μm in overview, and 2 μm or 0.5 μm in insets.
(F) Kinetochore architectures shown in (E) and their occurrence in MI oocytes treated as in (B). Data are from 55 metaphase-I oocytes (2 experiments). Error bars show SEM.
(G) Representative two sister kinetochores of a bivalent in control oocytes (left panel) or anti-Smc3 microinjected Trim-Away oocytes (other panels). Scale bars represent 0.5 μm.
Chromosomes (blue, Hoechst) and kinetochores (magenta, CREST) are shown in (B), (E), and (G). In (B) and (E), microtubules are additionally labeled (green, α-tubulin). p values are designated as **p < 0.01 and ****p < 0.0001. p values were calculated with one-way ANOVA followed by Tukey's test in (D) and Student's t test in (F). Arrows: white point to compact kinetochores, and yellow point to lobes within a fragmented MI kinetochore. Numbers in insets refer to sister kinetochores shown (as in the E schematic).
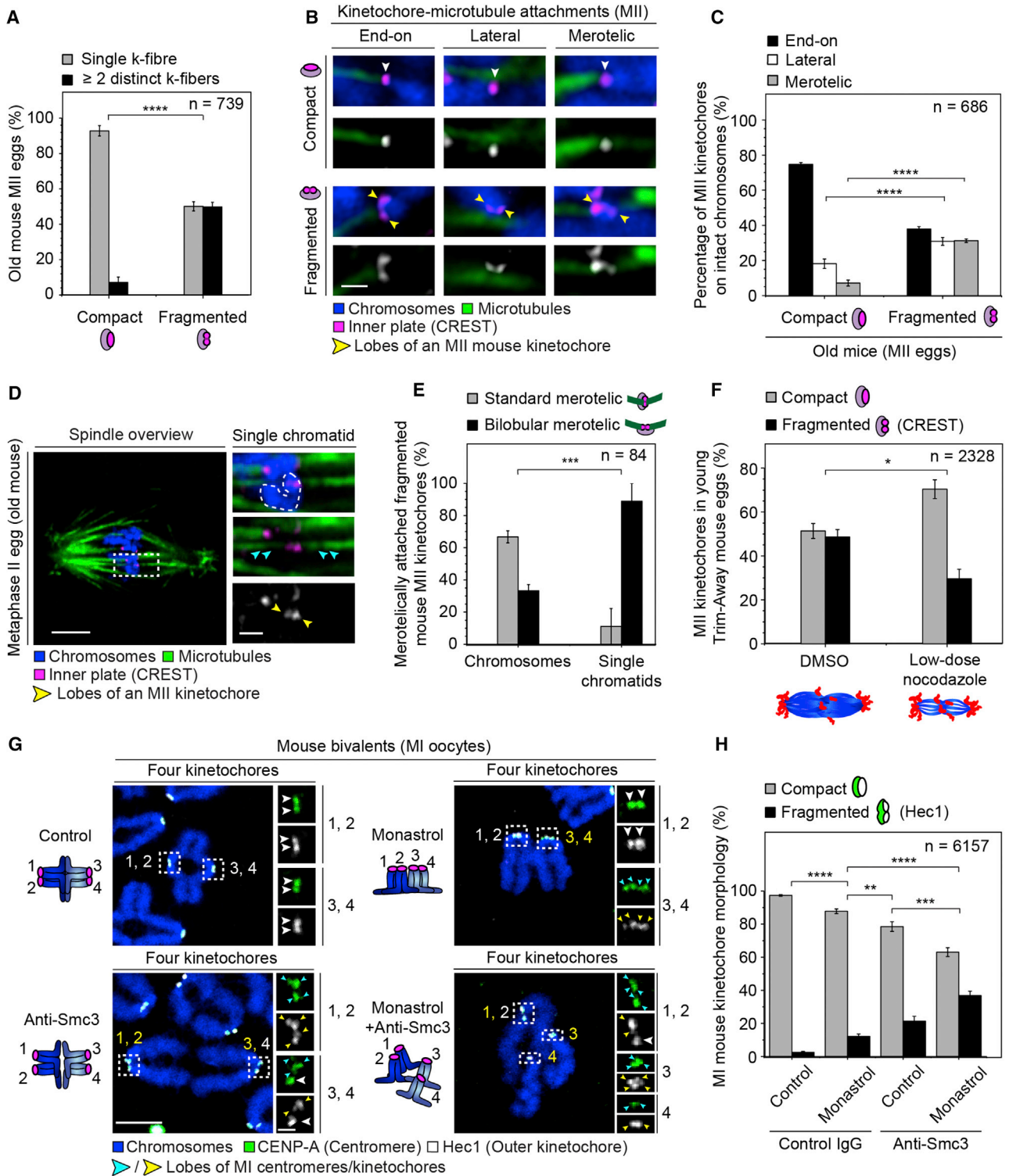See also Figure S6.

Figure 6. Fragmented Kinetochores Are More Likely to Be Abnormally Attached to Spindle Microtubules

(A) Quantification of the number of distinct k fibers attaching to compact/fragmented kinetochores at metaphase II (28 aged mouse MII eggs, 3 experiments) is shown.

(B) Representative kinetochore-microtubule attachment types, relative to the kinetochore fragmentation status. The scale bar represents 1 μm.

(C) Quantification of the microtubule attachment types shown in (B) across the specified MII kinetochore categories on intact chromosomes (28 aged mouse MII eggs, 3 experiments).

(legend continued on next page)

MTOC aggregate. Importantly, significantly more kinetochores became fragmented under conditions of monastrol treatment in anti-Smc3-injected oocytes, as compared to control monastrol-treated cells with intact cohesin (Figure 6H, second and fourth columns), which further supports our model that cohesin loss primes kinetochores for fragmentation. Together, these findings suggest that although meiotic kinetochores may have inherent structural properties that bias them toward a bilobular appearance, the emergence of two lobes is promoted by bidirectional pulling and grouping of kinetochore fragments by spindle microtubules.

DISCUSSION

Our study reveals that the internal architecture of centromeres and kinetochores in mammalian eggs changes as females age: centromeric chromatin decompacts and kinetochores fragment, which is linked to an increase in incorrect microtubule attachments. Acute removal of cohesin from centromeric regions is sufficient to reproduce these age-related changes in centromere and kinetochore architecture (Figure 7A). We therefore favor a model whereby kinetochore distortion starts at the level of centromeric chromatin: cohesin is gradually lost from centromeric regions as females age. This loss of cohesin leads to a broadening of centromeric chromatin and an expansion of associated kinetochores (Figure 7B). The expanded kinetochores are more likely to interact with multiple microtubule bundles and, if the bundles originate from distinct spindle poles (merotely), bidirectional pulling can have a further negative impact on kinetochore integrity. Age-related cohesin loss could thereby prime centromeres and the associated kinetochores to be attacked and altered by spindle microtubules.

Kinetochore fragmentation could contribute to the multifactorial [7–9, 23] age-related increase in aneuploidy in eggs. In support of this possibility, we detected significantly more abnormal lateral and merotelic spindle attachments in fragmented than in compact kinetochores in eggs from aged mice. Due to limited resolution in live-oocyte microscopy, we cannot currently follow how fragmented kinetochores segregate. However, merotelic attachments are well established to contribute to aneuploidy in mitosis [49]. Chromosomes with merotelically attached fragmented meiotic kinetochores could therefore mis-segregate in eggs as well. Cohesin loss may hence cause aneuploidy in

oocytes not only by leading to the premature dissociation of homologous chromosomes, sister chromatids, or sister kinetochores but also by priming kinetochores for fragmentation. We would still like to highlight that although cohesin loss was sufficient to induce changes to centromere and kinetochore morphology in eggs from young mice, multiple oocyte proteins deteriorate as females age [58] and may hence contribute to meiotic kinetochore fragmentation and the associated increase in abnormal kinetochore-microtubule attachments.

Assessing a woman's egg for kinetochore fragmentation may also help to assess the cohesin status of her oocyte pool in early stages of reproduction, because kinetochore fragmentation precedes the dissociation of chromosomes: we could already detect fragmented kinetochores in eggs from 34- to 36-week-old mice (Figure 2B), whereas dissociation of chromosomes into single chromatids only became prominent from 60 weeks onward (Figure S1A). Also in meiosis I, kinetochore fragmentation (Figure 5F) preceded the premature separation of the two homologous chromosomes within the bivalent (Figure 5C). These data therefore suggest that a loss of cohesin is first detectable at the level of the kinetochore before changes to the overall chromosome structure become evident, making kinetochore fragmentation an early readout of cohesin deterioration in aging oocytes.

Outer fibrous coronal regions of mitotic kinetochores were demonstrated to temporarily expand into a crescent before becoming stably bound by spindle microtubules [59–61]. However, these changes did not affect the centromere or inner kinetochore layers [59, 60], which is in contrast to meiotic kinetochore fragmentation that spans across multiple layers of the kinetochore complex and also affects stably bound chromosomes at the spindle equator. It will be interesting to investigate in future studies whether cohesin depletion also causes kinetochore fragmentation in mitotic cells. Following hypotonic treatment, mitotic kinetochores unravel into more than 80 distinct subunits [62], suggesting that they also have the potential to fragment. Although kinetochore stretching was previously artificially induced in maize meiocytes and mitotic cells [63–65], clear distortion is a rare event under wild-type conditions in unperturbed cells [49]. In contrast, our study demonstrates that a third of kinetochores exist in a clearly fragmented state in eggs from older females, making the bilobular appearance a prominent feature of the female meiotic kinetochore. Not only are cohesin

(legend on next page)

levels high but also spindle assembly in mitotic cells is much more rapid than in mammalian eggs [66], which could further explain why fragmentation is a rare event in mitosis. However, microtubule pulling could also play a role here, as some kinetochores lagging at anaphase onset also appeared bilobular when merotelic attachments were artificially increased [49].

Oocyte-specific spindle dynamics could contribute to fragmentation not only through direct pulling but also by influencing chromosome cohesion. Mammalian eggs only complete anaphase II upon fertilization [8, 67]. Thus, eggs frequently remain arrested in metaphase II for over 12 h, a phenomenon termed post-ovulatory aging [68]. Mitotic cells artificially halted at the metaphase stage undergo cohesion fatigue: cohesion becomes gradually insufficient and sister chromatids prematurely separate [69, 70]. Importantly, cohesion fatigue occurs only in the presence of microtubule pulling [69, 71]. Although it is clear that the major cohesin decline in mammalian oocytes occurs during prophase arrest [23], the physiological metaphase-II arrest that is unique to female meiosis could further reduce cohesion levels and thereby contribute to kinetochore fragmentation and sister chromatid splitting. In line with this idea, chromosome cohesion in MII eggs becomes occasionally insufficient to keep all chromatids together as the metaphase-II arrest endures [21, 72].

Several experiments in this study were based on a modified Trim-Away assay, which allowed us to partially deplete cohesins in oocytes and eggs from young mice. Using this assay, we were able to cause a partial dissociation of sister chromatids in young eggs, splitting of meiosis-I sister kinetochore pairs, as well as fragmentation of meiotic kinetochores, thus closely resembling the changes in chromosome and kinetochore architecture that occur during aging and have been attributed to a gradual loss of cohesin. Western blotting confirmed protein depletion from eggs, and immunofluorescence microscopy verified that our approach indeed removes cohesin from chromosomes. Due to technical limitations, as well as limited availability of antibodies to target Smc3 and Rec8 in oocytes, we only used one antibody against each cohesin complex subunit. However, the fact that the changes induced by targeting either Smc3 or Rec8 are consistent indicates that this approach is suitable to investigate the consequences of cohesin loss in mammalian oocytes and eggs.

The partial Trim-Away assay complements the previously developed mouse models heterozygous for cohesin genes [32], which induced low cohesin levels from the time the oocytes are first formed and allowed investigations into the effects of decreased cohesin levels on the early meiotic events that precede the protracted prophase arrest. The partial Trim-Away assay allows us to deplete cohesins in oocytes that were able to progress through the early stages of meiosis with normal cohesin levels, and is therefore suitable to study the effects of a late cohesin loss, similar to that occurring in oocytes from aged females, on meiotic chromosome and kinetochore architecture.

Notably, young mice used for the Trim-Away assays have considerably larger numbers of oocytes than aged females [19]. Thus, fewer animals are required to investigate the consequences of a partial loss of cohesin for meiosis, in comparison to the natural aging mouse model. In addition, these animals only need to be maintained for short periods of time, which reduces the number of cages that have to be kept. Importantly, the partial Trim-Away approach could also be applied to other proteins that only partially deteriorate during aging, and thus further contribute to our understanding of the maternal age effect in mammals.

STAR★METHODS

Detailed methods are provided in the online version of this paper and include the following:

- KEY RESOURCES TABLE
- LEAD CONTACT AND MATERIALS AVAILABILITY
- EXPERIMENTAL MODEL AND SUBJECT DETAILS
  - Primary mouse oocytes
  - Primary human oocytes
  - Primary pig oocytes
  - Cell culture
- METHOD DETAILS
  - Expression constructs and mRNA synthesis
  - Antibody microinjection
  - Drug addition experiments
  - Chromosome spreads
  - Cold-mediated microtubule depolymerization assays
  - Oocyte immunofluorescence
  - Immunofluorescence of tissue culture cells
  - Super-resolution immunofluorescence microscopy
  - Confocal microscopy in fixed cells
  - Confocal microscopy in live cells expressing fluorescent reporters or incubated with fluorescent dyes
  - Immunoblotting
- QUANTIFICATION AND STATISTICAL ANALYSIS
  - Chromosome counting and assessment of kinetochore configuration
  - Assessment of the effects of Trim-Away mediated cohesin loss on chromosome architecture in the metaphase of meiosis I
  - Modes of kinetochore-microtubule attachment
  - Quantification of fluorescence intensity of the centromeric cohesin pool
  - Quantification of western blot mean band intensity
  - Statistical analysis
- DATA AND CODE AVAILABILITY

SUPPLEMENTAL INFORMATION

Supplemental Information can be found online at https://doi.org/10.1016/j.cub.2019.09.006.

Figure 7. Age-Related Cohesin Loss Alters Chromosome Architecture and Fragments Mammalian Meiotic Kinetochores into Distinct Lobes
Scheme summarizing how cohesin loss affects not only sister kinetochore pairing but also the internal kinetochore architecture in meiosis-I oocytes and meiosis-II eggs (A), and a model proposing how cohesin-dependent changes in centromeric architecture may promote the fragmentation of a meiotic kinetochore into lobes (B).

AUTHOR CONTRIBUTIONS

A.P.Z. and M.S. conceived the project, designed the experiments, and wrote the manuscript. A.P.Z. performed and analyzed all experiments with the following exceptions: E.B. performed the experiments and analyzed the data in Figures S2B and S3A–S3C; N.S. performed the experiments and analyzed the data in Figures S1C, S3D, and S3E; A.-S.F. analyzed the data in Figures 1I, 1J, S2D, and 3E and immunolabeled/imaged the spreads from the Trim-Away experiments shown in Figures 3C, 3J, S4B, and S5A. J.R.G. and E.R.H. provided the data for Figure S6A. M.B., K.E., H.E., and R.M. supervised the collection of human oocytes at the IVF clinics. K.B.S. and A.P.Z. cultured and subsequently fixed the human oocytes used in this study. A.P.Z. prepared the figures and schematic diagrams for the manuscript. All authors commented on the manuscript. M.S. supervised the study.

DECLARATION OF INTERESTS

The authors declare no competing interests.

REFERENCES

1. Black, B.E., and Bassett, E.A. (2008). The histone variant CENP-A and centromere specification. Curr. Opin. Cell Biol. *20*, 91–100.

2. Cheeseman, I.M. (2014). The kinetochore. Cold Spring Harb. Perspect. Biol. *6*, a015826.

3. Pesenti, M.E., Weir, J.R., and Musacchio, A. (2016). Progress in the structural and functional characterization of kinetochores. Curr. Opin. Struct. Biol. *37*, 152–163.

4. Pereira, A.J., and Maiato, H. (2012). Maturation of the kinetochore-microtubule interface and the meaning of metaphase. Chromosome Res. *20*, 563–577.

5. Auckland, P., and McAinsh, A.D. (2015). Building an integrated model of chromosome congression. J. Cell Sci. *128*, 3363–3374.

6. Amargant, F., Barragan, M., Vassena, R., and Vernos, I. (2019). Insights of the tubulin code in gametes and embryos: from basic research to potential clinical applications in humans. Biol. Reprod *100*, 575–589.

7. Nagaoka, S.I., Hassold, T.J., and Hunt, P.A. (2012). Human aneuploidy: mechanisms and new insights into an age-old problem. Nat. Rev. Genet. *13*, 493–504.

8. Herbert, M., Kalleas, D., Cooney, D., Lamb, M., and Lister, L. (2015). Meiosis and maternal aging: insights from aneuploid oocytes and trisomy births. Cold Spring Harb. Perspect. Biol. *7*, a017970.

9. Webster, A., and Schuh, M. (2017). Mechanisms of aneuploidy in human eggs. Trends Cell Biol. *27*, 55–68.

10. Santaguida, S., and Musacchio, A. (2009). The life and miracles of kinetochores. EMBO J. *28*, 2511–2531.

11. Hodges, C.A., Revenkova, E., Jessberger, R., Hassold, T.J., and Hunt, P.A. (2005). SMC1beta-deficient female mice provide evidence that cohesins are a missing link in age-related nondisjunction. Nat. Genet. *37*, 1351–1355.

12. Chiang, T., Duncan, F.E., Schindler, K., Schultz, R.M., and Lampson, M.A. (2010). Evidence that weakened centromere cohesion is a leading cause of age-related aneuploidy in oocytes. Curr. Biol. *20*, 1522–1528.

13. Lister, L.M., Kouznetsova, A., Hyslop, L.A., Kalleas, D., Pace, S.L., Barel, J.C., Nathan, A., Floros, V., Adelfalk, C., Watanabe, Y., et al. (2010). Age-related meiotic segregation errors in mammalian oocytes are preceded by depletion of cohesin and Sgo2. Curr. Biol. *20*, 1511–1521.

14. Shomper, M., Lappa, C., and FitzHarris, G. (2014). Kinetochore microtubule establishment is defective in oocytes from aged mice. Cell Cycle *13*, 1171–1179.

15. Danylevska, A., Kovacovicova, K., Awadova, T., and Anger, M. (2014). The frequency of precocious segregation of sister chromatids in mouse female meiosis I is affected by genetic background. Chromosome Res. *22*, 365–373.

16. Sakakibara, Y., Hashimoto, S., Nakaoka, Y., Kouznetsova, A., Höög, C., and Kitajima, T.S. (2015). Bivalent separation into univalents precedes age-related meiosis I errors in oocytes. Nat. Commun. *6*, 7550.

17. Zielinska, A.P., Holubcova, Z., Blayney, M., Elder, K., and Schuh, M. (2015). Sister kinetochore splitting and precocious disintegration of bivalents could explain the maternal age effect. eLife *4*, e11389.

18. Patel, J., Tan, S.L., Hartshorne, G.M., and McAinsh, A.D. (2015). Unique geometry of sister kinetochores in human oocytes during meiosis I may explain maternal age-associated increases in chromosomal abnormalities. Biol. Open *5*, 178–184.

19. Merriman, J.A., Jennings, P.C., McLaughlin, E.A., and Jones, K.T. (2012). Effect of aging on superovulation efficiency, aneuploidy rates, and sister chromatid cohesion in mice aged up to 15 months. Biol. Reprod. *86*, 49.

20. Duncan, F.E., Hornick, J.E., Lampson, M.A., Schultz, R.M., Shea, L.D., and Woodruff, T.K. (2012). Chromosome cohesion decreases in human eggs with advanced maternal age. Aging Cell *11*, 1121–1124.

21. Yun, Y., Lane, S.I., and Jones, K.T. (2014). Premature dyad separation in meiosis II is the major segregation error with maternal age in mouse oocytes. Development *141*, 199–208.

22. Lagirand-Cantaloube, J., Ciabrini, C., Charrasse, S., Ferrieres, A., Castro, A., Anahory, T., and Lorca, T. (2017). Loss of centromere cohesion in aneuploid human oocytes correlates with decreased kinetochore localization of the Sac proteins Bub1 and Bubr1. Sci. Rep. *7*, 44001.

23. Jessberger, R. (2012). Age-related aneuploidy through cohesion exhaustion. EMBO Rep. *13*, 539–546.

24. Parisi, S., McKay, M.J., Molnar, M., Thompson, M.A., van der Spek, P.J., van Drunen-Schoenmaker, E., Kanaar, R., Lehmann, E., Hoeijmakers, J.H., and Kohli, J. (1999). Rec8p, a meiotic recombination and sister chromatid cohesion phosphoprotein of the Rad21p family conserved from fission yeast to humans. Mol. Cell. Biol. *19*, 3515–3528.

25. Prieto, I., Suja, J.A., Pezzi, N., Kremer, L., Martínez-A, C., Rufas, J.S., and Barbero, J.L. (2001). Mammalian STAG3 is a cohesin specific to sister chromatid arms in meiosis I. Nat. Cell Biol. *3*, 761–766.

26. Revenkova, E., Eijpe, M., Heyting, C., Gross, B., and Jessberger, R. (2001). Novel meiosis-specific isoform of mammalian SMC1. Mol. Cell. Biol. *21*, 6984–6998.

27. Tachibana-Konwalski, K., Godwin, J., van der Weyden, L., Champion, L., Kudo, N.R., Adams, D.J., and Nasmyth, K. (2010). Rec8-containing

cohesin maintains bivalents without turnover during the growing phase of mouse oocytes. Genes Dev. *24*, 2505–2516.

28. Petronczki, M., Siomos, M.F., and Nasmyth, K. (2003). Un ménage à quatre: the molecular biology of chromosome segregation in meiosis. Cell *112*, 423–440.

29. Burkhardt, S., Borsos, M., Szydlowska, A., Godwin, J., Williams, S.A., Cohen, P.E., Hirota, T., Saitou, M., and Tachibana-Konwalski, K. (2016). Chromosome cohesion established by Rec8-cohesin in fetal oocytes is maintained without detectable turnover in oocytes arrested for months in mice. Curr. Biol. *26*, 678–685.

30. Liu, L., and Keefe, D.L. (2008). Defective cohesin is associated with age-dependent misaligned chromosomes in oocytes. Reprod. Biomed. Online *16*, 103–112.

31. Angell, R. (1997). First-meiotic-division nondisjunction in human oocytes. Am. J. Hum. Genet. *61*, 23–32.

32. Murdoch, B., Owen, N., Stevense, M., Smith, H., Nagaoka, S., Hassold, T., McKay, M., Xu, H., Fu, J., Revenkova, E., et al. (2013). Altered cohesin gene dosage affects mammalian meiotic chromosome structure and behavior. PLoS Genet. *9*, e1003241.

33. Kuliev, A., Zlatopolsky, Z., Kirillova, I., Spivakova, J., and Cieslak Janzen, J. (2011). Meiosis errors in over 20,000 oocytes studied in the practice of preimplantation aneuploidy testing. Reprod. Biomed. Online *22*, 2–8.

34. Fragouli, E., Alfarawati, S., Spath, K., Jaroudi, S., Sarasa, J., Enciso, M., and Wells, D. (2013). The origin and impact of embryonic aneuploidy. Hum. Genet. *132*, 1001–1013.

35. Hou, Y., Fan, W., Yan, L., Li, R., Lian, Y., Huang, J., Li, J., Xu, L., Tang, F., Xie, X.S., and Qiao, J. (2013). Genome analyses of single human oocytes. Cell *155*, 1492–1506.

36. Ottolini, C.S., Newnham, L., Capalbo, A., Natesan, S.A., Joshi, H.A., Cimadomo, D., Griffin, D.K., Sage, K., Summers, M.C., Thornhill, A.R., et al. (2015). Genome-wide maps of recombination and chromosome segregation in human oocytes and embryos show selection for maternal recombination rates. Nat. Genet. *47*, 727–735.

37. Das, A., Smoak, E.M., Linares-Saldana, R., Lampson, M.A., and Black, B.E. (2017). Centromere inheritance through the germline. Chromosoma *126*, 595–604.

38. Watanabe, Y. (2012). Geometry and force behind kinetochore orientation: lessons from meiosis. Nat. Rev. Mol. Cell Biol. *13*, 370–382.

39. Smoak, E.M., Stein, P., Schultz, R.M., Lampson, M.A., and Black, B.E. (2016). Long-term retention of CENP-A nucleosomes in mammalian oocytes underpins transgenerational inheritance of centromere identity. Curr. Biol. *26*, 1110–1116.

40. Hell, S.W., and Wichmann, J. (1994). Breaking the diffraction resolution limit by stimulated emission: stimulated-emission-depletion fluorescence microscopy. Opt. Lett. *19*, 780–782.

41. Earnshaw, W.C., and Rothfield, N. (1985). Identification of a family of human centromere proteins using autoimmune sera from patients with scleroderma. Chromosoma *91*, 313–321.

42. Tsutsumi, M., Fujiwara, R., Nishizawa, H., Ito, M., Kogo, H., Inagaki, H., Ohye, T., Kato, T., Fujii, T., and Kurahashi, H. (2014). Age-related decrease of meiotic cohesins in human oocytes. PLoS ONE *9*, e96710.

43. Clift, D., McEwan, W.A., Labzin, L.I., Konieczny, V., Mogessie, B., James, L.C., and Schuh, M. (2017). A method for the acute and rapid degradation of endogenous proteins. Cell *171*, 1692–1706.e18.

44. Uhlmann, F. (2004). The mechanism of sister chromatid cohesion. Exp. Cell Res. *296*, 80–85.

45. Watanabe, Y., and Nurse, P. (1999). Cohesin Rec8 is required for reductional chromosome segregation at meiosis. Nature *400*, 461–464.

46. Klein, F., Mahr, P., Galova, M., Buonomo, S.B., Michaelis, C., Nairz, K., and Nasmyth, K. (1999). A central role for cohesins in sister chromatid cohesion, formation of axial elements, and recombination during yeast meiosis. Cell *98*, 91–103.

47. Eijpe, M., Offenberg, H., Jessberger, R., Revenkova, E., and Heyting, C. (2003). Meiotic cohesin REC8 marks the axial elements of rat

synaptonemal complexes before cohesins SMC1beta and SMC3. J. Cell Biol. *160*, 657–670.

48. Salmon, E.D., and Begg, D.A. (1980). Functional implications of cold-stable microtubules in kinetochore fibers of insect spermatocytes during anaphase. J. Cell Biol. *85*, 853–865.

49. Cimini, D., Howell, B., Maddox, P., Khodjakov, A., Degrassi, F., and Salmon, E.D. (2001). Merotelic kinetochore orientation is a major mechanism of aneuploidy in mitotic mammalian tissue cells. J. Cell Biol. *153*, 517–527.

50. Kouznetsova, A., Hernández-Hernández, A., and Höög, C. (2014). Merotelic attachments allow alignment and stabilization of chromatids in meiosis II oocytes. Nat. Commun. *5*, 4409.

51. Cheng, J.M., Li, J., Tang, J.X., Hao, X.X., Wang, Z.P., Sun, T.C., Wang, X.X., Zhang, Y., Chen, S.R., and Liu, Y.X. (2017). Merotelic kinetochore attachment in oocyte meiosis II causes sister chromatids segregation errors in aged mice. Cell Cycle *16*, 1404–1413.

52. Schuh, M., and Ellenberg, J. (2007). Self-organization of MTOCs replaces centrosome function during acentrosomal spindle assembly in live mouse oocytes. Cell *130*, 484–498.

53. Nakagawa, S., and FitzHarris, G. (2017). Intrinsically defective microtubule dynamics contribute to age-related chromosome segregation errors in mouse oocyte meiosis-I. Curr. Biol. *27*, 1040–1047.

54. Holubcová, Z., Blayney, M., Elder, K., and Schuh, M. (2015). Human oocytes. Error-prone chromosome-mediated spindle assembly favors chromosome segregation defects in human oocytes. Science *348*, 1143–1147.

55. Haverfield, J., Dean, N.L., Nöel, D., Rémillard-Labrosse, G., Paradis, V., Kadoch, I.J., and FitzHarris, G. (2017). Tri-directional anaphases as a novel chromosome segregation defect in human oocytes. Hum. Reprod. *32*, 1293–1303.

56. Ashar, H.R., James, L., Gray, K., Carr, D., Black, S., Armstrong, L., Bishop, W.R., and Kirschmeier, P. (2000). Farnesyl transferase inhibitors block the farnesylation of CENP-E and CENP-F and alter the association of CENP-E with the microtubules. J. Biol. Chem. *275*, 30451–30457.

57. Clift, D., and Schuh, M. (2015). A three-step MTOC fragmentation mechanism facilitates bipolar spindle assembly in mouse oocytes. Nat. Commun. *6*, 7217.

58. Schwarzer, C., Siatkowski, M., Pfeiffer, M.J., Baeumer, N., Drexler, H.C., Wang, B., Fuellen, G., and Boiani, M. (2014). Maternal age effect on mouse oocytes: new biological insight from proteomic analysis. Reproduction *148*, 55–72.

59. Hoffman, D.B., Pearson, C.G., Yen, T.J., Howell, B.J., and Salmon, E.D. (2001). Microtubule-dependent changes in assembly of microtubule motor proteins and mitotic spindle checkpoint proteins at PtK1 kinetochores. Mol. Biol. Cell *12*, 1995–2009.

60. Magidson, V., Paul, R., Yang, N., Ault, J.G., O'Connell, C.B., Tikhonenko, I., McEwen, B.F., Mogilner, A., and Khodjakov, A. (2015). Adaptive changes in the kinetochore architecture facilitate proper spindle assembly. Nat. Cell Biol. *17*, 1134–1144.

61. Sacristan, C., Ahmad, M.U.D., Keller, J., Fermie, J., Groenewold, V., Tromer, E., Fish, A., Melero, R., Carazo, J.M., Klumperman, J., et al. (2018). Dynamic kinetochore size regulation promotes microtubule capture and chromosome biorientation in mitosis. Nat. Cell Biol. *20*, 800–810.

62. Zinkowski, R.P., Meyne, J., and Brinkley, B.R. (1991). The centromere-kinetochore complex: a repeat subunit model. J. Cell Biol. *113*, 1091–1110.

63. Khodjakov, A., Cole, R.W., McEwen, B.F., Buttle, K.F., and Rieder, C.L. (1997). Chromosome fragments possessing only one kinetochore can congress to the spindle equator. J. Cell Biol. *136*, 229–240.

64. Yu, H.G., and Dawe, R.K. (2000). Functional redundancy in the maize meiotic kinetochore. J. Cell Biol. *151*, 131–142.

65. Drpic, D., Pereira, A.J., Barisic, M., Maresca, T.J., and Maiato, H. (2015). Polar ejection forces promote the conversion from lateral to end-on

kinetochore-microtubule attachments on mono-oriented chromosomes. Cell Rep. *13*, 460–468.

66. Ohkura, H. (2015). Meiosis: an overview of key differences from mitosis. Cold Spring Harb. Perspect. Biol. *7*, a015859.

67. Clift, D., and Schuh, M. (2013). Restarting life: fertilization and the transition from meiosis to mitosis. Nat. Rev. Mol. Cell Biol. *14*, 549–562.

68. Wilcox, A.J., Weinberg, C.R., and Baird, D.D. (1998). Post-ovulatory ageing of the human oocyte and embryo failure. Hum. Reprod. *13*, 394–397.

69. Daum, J.R., Potapova, T.A., Sivakumar, S., Daniel, J.J., Flynn, J.N., Rankin, S., and Gorbsky, G.J. (2011). Cohesion fatigue induces chromatid separation in cells delayed at metaphase. Curr. Biol. *21*, 1018–1024.

70. Stevens, D., Gassmann, R., Oegema, K., and Desai, A. (2011). Uncoordinated loss of chromatid cohesion is a common outcome of extended metaphase arrest. PLoS ONE *6*, e22969.

71. Sapkota, H., Wasiak, E., Daum, J.R., and Gorbsky, G.J. (2018). Multiple determinants and consequences of cohesion fatigue in mammalian cells. Mol. Biol. Cell *29*, 1811–1824.

72. Steuerwald, N.M., Steuerwald, M.D., and Mailhes, J.B. (2005). Post-ovulatory aging of mouse oocytes leads to decreased MAD2 transcripts and increased frequencies of premature centromere separation and anaphase. Mol. Hum. Reprod. *11*, 623–630.

73. Bucevičius, J., Keller-Findeisen, J., Gilat, T., Hell, S.W., and Lukinavičius, G. (2018). Rhodamine-Hoechst positional isomers for highly efficient staining of heterochromatin. Chem. Sci. (Camb.) *10*, 1962–1970.

74. Liman, E.R., Tytgat, J., and Hess, P. (1992). Subunit stoichiometry of a mammalian K^+ channel determined by construction of multimeric cDNAs. Neuron *9*, 861–871.

75. Mogessie, B., and Schuh, M. (2017). Actin protects mammalian eggs against chromosome segregation errors. Science *357*, eaal1647.

76. Zielinska, A.P., and Schuh, M. (2018). A microscopy-based approach for studying meiosis in live and fixed human oocytes. Methods Cell Biol. *145*, 315–333.

77. Jaffe, L.A., Norris, R.P., Freudzon, M., Ratzan, W.J., and Mehlmann, L.M. (2009). Microinjection of follicle-enclosed mouse oocytes. Methods Mol. Biol. *518*, 157–173.

78. Silva, M.C.C., Wutz, G., Tachibana, K., and Peters, J.M. (2018). Analysis of chromosomes from mouse oocytes and mammalian cultured cells by light microscopy. Methods Cell Biol. *144*, 287–305.

STAR★METHODS

KEY RESOURCES TABLE

REAGENT or RESOURCE	SOURCE	IDENTIFIER
Antibodies		
Rabbit anti-Rec8	Produced in-house	Epitope based on [47]
Rat anti-α-Tubulin	Bio-Rad	MCA78G; RRID:AB_325005
CREST serum	Antibodies Incorporated	15-234-0001; RRID: AB_2687472
CREST serum	Europa Bioproducts	FZ90C- CS1058
Rabbit anti-Smc3	Abcam	ab9263; RRID:AB_307122
Rabbit anti-Smc3	Abcam	EPR7984; RRID:AB_11150430
Mouse anti-Hec1	Santa Cruz	sc-135934; RRID:AB_2149754
Mouse anti-Hec1	Abcam	ab3613; RRID:AB_303949
Rabbit anti-CENP-A	Cell Signaling	2048; RRID:AB_1147629
Rabbit anti-CENP-F	Abcam	ab5; RRID:AB_304721
Mouse anti-CENP-C	Abcam	ab50974; RRID:AB_869095
Sheep anti-BubR1	Abcam	ab28192; RRID:AB_725785
Rabbit anti-Smc3	Bethyl Laboratories	A300-060A; RRID:AB_67579
Normal Rabbit IgG	Millipore	12-370; RRID:AB_145841
Goat anti-Rabbit IgG (H+L) Highly Cross-Adsorbed Secondary Antibody, Alexa Fluor 488	ThermoFisher	A11034; RRID:AB_2576217
Goat anti-Human IgG (H+L) Cross-Adsorbed Secondary Antibody, Alexa Fluor 488	ThermoFisher	A11013; RRID:AB_2534080
Chicken anti-Rat IgG (H+L) Cross-Adsorbed Secondary Antibody, Alexa Fluor 647	ThermoFisher	A21472; RRID:AB_2535875
Goat anti-Mouse IgG (H+L) Cross-Adsorbed Secondary Antibody, Alexa Fluor 546	ThermoFisher	A11003; RRID:AB_2534071
Donkey anti-Rabbit IgG (H+L) Highly Cross-Adsorbed Secondary Antibody, Alexa Fluor 647	ThermoFisher	A31573; RRID:AB_2536183
Goat anti-Rabbit IgG (H+L) Cross-Adsorbed Secondary Antibody, HRP	ThermoFisher	31462; RRID:AB_228338
Goat anti-Rat IgG Secondary Antibody, HRP	Santa Cruz	sc-2032; RRID:AB_631755
Goat anti-Rabbit STAR RED	Abberior	2-0012-011-9; RRID: AB_2620152
Goat anti-Mouse Alexa594-conjugated	ThermoFisher	R37121; RRID:AB_2556549
Chemicals, Peptides, and Recombinant Proteins		
Hoechst 33342	ThermoFisher	H3570; RRID:AB_2651133
PicoGreen	ThermoFisher	P11496
SiR-tubulin	Spirochrome	CHF420.00
5-TMR-Hoechst	N/A	Gift from Grazvydas Lukinavičius (see also [73])
dbcAMP (N6,2′-O-Dibutyryladenosine 3′,5′-cyclic monophosphate sodium salt)	Sigma	D0627
Nocodazole	Sigma	M1404
Monastrol	Sigma	M8515
Hyaluronidase	Sigma	H4272
NP-40 Alternative	Merck	492016
Critical Commercial Assays		
mMESSAGE mMACHINE T7 Transcription Kit	ThermoFisher	AM1334
SuperSignal West Femto Maximum Sensitivity Substrate	ThermoFisher	34095
SNAP-Cell Starter Kit	New England Biolabs	E9100S
Lambda Protein Phosphatase (Lambda PP)	New England Biolabs	P0753S

Continued

REAGENT or RESOURCE	SOURCE	IDENTIFIER
Experimental Models: Organisms/Strains		
Mouse: FVB/N	Charles River Janvier	RRID:IMSR_CRL:207
Human oocytes	IVF clinics	N/A
Pig ovaries (*Sus scrofa domesticus*)	Local slaughterhouse	N/S
NIH 3T3	ATCC	CRL-1658
HEK293T	ATCC	CRL-3216
Recombinant DNA		
pGEMHE	Jan Ellenberg	[74]
pGEMHE-*H2B*-mRFP	Jan Ellenberg	[52]
pGEMHE-EGFP-*Map4*	Jan Ellenberg	[52]
pGEMHE-SNAP-MAP4-MTBD	Melina Schuh	[75]
pGEMHE-CENPB-mEmerald	This paper	N/A
pGEMHE-TRIM21	Melina Schuh	[43]
CENPB-mEmerald	Addgene	54037
Software and Algorithms		
OriginPro 2016G	OriginLab	N/A
ImageJ	N/A	N/A
Imaris	BITPLANE	N/A
AiryScan Processing Algorithm	Zeiss	N/A

LEAD CONTACT AND MATERIALS AVAILABILITY

All unique/stable reagents generated in this study are available from the Lead Contact (Melina Schuh, melina.schuh@mpibpc.mpg.de) with a completed Materials Transfer Agreement.

EXPERIMENTAL MODEL AND SUBJECT DETAILS

Primary mouse oocytes

Female FVB/N mice (6-8 weeks) were obtained directly from Janvier or from an in-house breeding colony that was generated using mice purchased from Charles River. For aging studies, 35-120 week old mice were used. All mice were maintained in a specific pathogen-free environment, according to the guidelines of the MPI-bpc animal facility. The experiments involving mice have been performed in compliance with the German Law on Animal Welfare.

Oocytes were collected from ovaries of 6-8 or 35-120 week old FVB/N mice and cultured at 37°C under mineral oil in homemade M2 medium supplemented with 250 μM dbcAMP (Sigma; D0627) to maintain the prophase arrest. To trigger resumption of meiosis, oocytes were release into dbcAMP-free medium. Oocytes from the FVB/N strain require the following amounts of time after release from prophase arrest (NEBD, nuclear envelope breakdown) to complete key meiotic events: 6 h 30 min to stably align all chromosomes at the metaphase plate of meiosis I and 8 h 30 min to undergo anaphase I (Figure S2B). Therefore, to study chromosome and kinetochore architecture in steady-state MII eggs that have reached final metaphase-II arrest, we fixed the oocytes 16 h after release into dbcAMP-free medium. In the few experiments where we investigated meiosis I chromosome and kinetochore architectures, we preserved the oocytes 7 h 15 min – 8 hours after release from prophase arrest.

Primary human oocytes

All human oocytes used in this study were sourced from women undergoing assisted reproduction treatments after having obtained fully informed consent. The use of immature unfertilized human oocytes has been approved by the UK's National Research Ethics Service under the REC reference 11/EE/0346 (IRAS Project ID 84952), the Ethics Committee of Lower Saxony (Ärtzekammer Niedersachsen) under the reference 15/2016 and the Danish Capital Region's Ethics Committee (H-16044731). The unfertilized oocytes were donated by patients at Bourn Hall Clinic (Cambridge, UK) between January 2016 and March 2018, at Kinderwunschzentrum (Göttingen, Germany) between September 2016 and March 2018, at the Laboratory for Reproductive Biology, Capital Region H hospitals (Copenhagen, Denmark) and INVICTA Fertility Clinic (Gdansk, Poland) between January 2016 and April 2018. 48 meiosis II eggs from 34 donors were included in the analysis. The donors were aged between 19 and 45 years and underwent ovarian stimulation for intracytoplasmic sperm injection (ICSI). Only oocytes that were immature and hence unsuitable for the ICSI procedure were designated to the study. None of the oocytes used in this study were freeze-thawed. Oocytes were cultured as previously described [76].

In brief, following retrieval, oocytes were transported to the research lab and cultured in G-MOPS medium (Vitrolife, #10129) supplemented with 10% FBS (GIBCO, #16000044) under mineral oil (Merck, #8012-95-1) at 37°C. Only oocytes that appeared morphologically healthy and underwent NEBD within 24 hours from retrieval were included in the study. The developmental stage of the oocyte was assessed either manually by scoring for the presence of the germinal vesicle at 60 minute intervals or using a Primo Vision Evo+ timelapse camera installed inside the incubator. To analyze chromosome and kinetochore morphology at metaphase-II, the oocytes were fixed 4-9 hours after polar body extrusion.

Primary pig oocytes

Porcine ovaries were obtained from a local slaughterhouse and transported to the laboratory within 45 minutes of retrieval in a portable 37°C incubator in M2 medium supplemented with 1 mM dbcAMP. In brief, the oocytes were retrieved by aspiration of the large antral follicles with an 18-gauge needle affixed to a 1 mL disposable syringe. The fluid aspirated was then transferred to dishes containing 1 mL of M2 medium supplemented with dbcAMP and the cumulus-oocyte complexes (COC) were collected from the sediment. The COCs were then washed extensively to remove the cellular debris and transferred to droplets of M2+dbcAMP under mineral oil. Only large oocytes with homogeneous cytoplasm and surrounded by several layers of compact cumulus cells were selected for experiments. Oocytes dedicated to immunolabelling at the metaphase-II stage were released into dbcAMP-free medium and cultured for 30 hours in a 37.5°C incubator prior to fixation.

Cell culture

NIH 3T3 and HEK293T cells (ATCC) were cultured in DMEM (GIBCO; 31966021) supplemented with 10% Calf Serum (Sigma; C8056) and penicillin-streptomycin at 37°C in a 5% CO_2 humidified atmosphere and regularly checked to be mycoplasma-free.

METHOD DETAILS

Expression constructs and mRNA synthesis

Capped mRNA was synthesized with T7 RNA polymerase (mMessage mMachine Kit Ambion), precipitated with isopropanol, and dissolved in 6 μL of RNase-free water. The following constructs were used: pGEMHE-EGFP-*MAP4* and pGEMHE-SNAP-*MAP4-MTBD* (aa659-1125 of the microtubule binding domain of MAP4) to label microtubules, pGEMHE-*H2B*-mRFP to label the chromosomes, pGEMHE-*CENPB*-mEmerald to label kinetochores and pGEMHE-TRIM21 [43] to overexpress the mouse variant of the TRIM21 protein in the oocytes. To generate the kinetochore labeling construct, *CENPB*-mEmerald (Addgene, 54037) was subcloned into pGEMHE vector using the NheI and NotI restrictions sites, while other expression constructs were previously described. Quantitative microinjection was performed as outlined previously [77]. After injection of mRNAs into oocytes, the oocytes were incubated for 3 hours at 37°C to express the protein.

Antibody microinjection

The anti-Smc3 antibody used was rabbit anti-Smc3 (Abcam ab9263). The anti-Rec8 antibody was generated in-house using a previously characterized epitope [47]. The control IgG used was a normal rabbit IgG (Millipore 12-370). With the exception of anti-Smc3, all antibodies were concentrated using Amicon Ultra-0.5 100 kDa centrifugal filter devices (Millipore) to remove traces of azide and replace the buffer with PBS. Following concentrations of antibodies were used: anti-Smc3 (1 mg/ml), anti-Rec8 (2 mg/ml) and control IgG (2 mg/ml). Prior to microinjection into eggs, the antibodies were spun at 10,000 rpm (4°C) for 10 minutes and supplemented with NP-40 at a final concentration of 0.05%. Antibody microinjection into eggs was performed as described previously for mRNA microinjection [52]. For full depletion experiments in the metaphase of meiosis II, a bolus of 6 pl of anti-Smc3 or anti-Rec8 was microinjected into the eggs, whereas for partial depletion experiments 2 pl of the anti-Smc3 antibody were microinjected. For partial depletion of cohesins in meiosis I, a bolus of 4 pl of the anti-Smc3 antibody was microinjected 4.5-5.5 hours after the oocytes were released from prophase arrest. The oocytes were then fixed 7 h 15 min – 8 hours after the release.

Drug addition experiments

To assess the acute effects of drugs on chromosome and kinetochore morphologies, oocytes were matured in M2 medium until they reached meiosis II and were washed into drug containing medium immediately before imaging. To partially depolymerize microtubules, TRIM-expressing eggs were treated with 50 nM nocodazole (Sigma) before the introduction of anti-cohesin antibodies. No more than 5 eggs were microinjected with the antibody at a time, to minimize the interval between cohesin degradation and exposure to the drug-free medium. The changes in microtubule dynamics were assessed live on the microscope.

In order to prevent spindle bipolarization, TRIM21-overexpressing oocytes were released from the dbcAMP-induced arrest into M2 medium containing 150 μM of monastrol (Sigma). The oocytes were incubated in the drug-containing medium from release until the chromosome spreading procedure. 5 hours after the release, the MI oocytes were microinjected with a bolus of 4 pl of an anti-Smc3 antibody (1 mg/ml in PBS) or control IgG. Subsequently, they were placed on a microscope to assess chromosome organization. After additional 3 hours, chromosome spreading procedure was performed.

All drug experiments included appropriate DMSO control groups.

Chromosome spreads

Oocytes were transferred through droplets of acidic Tyrode's solution (pH 2.5) at 37°C to remove the zona pellucidae. After subsequent 14 min incubation in 1:1 FBS:water at 37°C, oocytes were fixed on a glass slide in a drop of 1% paraformaldehyde, supplemented with 0.15% Triton X-100 and 3 mM DTT [78]. For human oocyte spreads, as bursting of human MI oocytes is more variable, the oocytes were allowed to swell in a drop of 0.9% sodium citrate (w/v) prior to transfer to the formaldehyde solution. Glass slides were stored in a humidified chamber at room temperature overnight. In experiments where kinetochore architecture was assessed, following air-drying the oocytes were incubated the next morning with primary antibodies (mouse anti-Hec1, Santa Cruz sc-135934, 1:100; rabbit anti-CENP-A, Cell Signaling C51A7 1, 1:100; human ACA centromere CREST autoantibody, Antibodies Incorporated 15-234-0001, 1:100; mouse anti-CENP-C, ab50974, 1:20; sheep anti-BubR1, ab28192, 1:20) for 1 h at 37°C or overnight at RT. For AiryScan microscopy, appropriate Alexa488/546 conjugated secondary antibodies raised in goat (ThermoFisher, 1:200) were used for visualization. 1 μg/ml Hoechst was applied for DNA counterstaining. Samples for STED microscopy were counterstained with PicoGreen (ThermoFisher, 1:100) for 2h at room temperature to visualize the DNA, prior to incubation with the following secondary antibodies: STAR RED goat anti-rabbit (Abberior, 1:400) and Alexa594-conjugated goat anti-mouse (ThermoFisher, 1:200). In cases where anti-CENP-A antibody was used to visualize the centromeres, oocytes were treated for 30 min with Lambda Protein Phosphatase at 30°C prior to antibody incubation, as described previously [39].

In experiments where the fluorescence signal intensity of the centromeric pool of cohesin complexes was compared between control and Trim-Away eggs, slides were air-dried and subsequently incubated at 4°C with human CREST serum (1:250, Europa Bioproducts, FZ90C- CS1058) and an in-house anti-Rec8 antibody (1:100, epitope based on Eijpe et al., 2003 [47]) or an anti-Smc3 antibody (rabbit anti-Smc3, Bethyl Laboratories, A300-060A) overnight. Next morning, the slides were incubated for 1h at RT with the following secondary antibodies: donkey anti-rabbit 488 and goat anti-human 546/647 (ThermoFischer, 1:200). Additionally, the DNA was visualized with 40 μM Hoechst.

Cold-mediated microtubule depolymerization assays

To determine k-fiber stability and kinetochore-microtubule attachment modes, non-kinetochore-bound microtubules were selectively depolymerized by exposing the eggs to 4°C. The durations of the cold-treatments to obtain an optimal microtubule density were adapted as follows: 6 minutes for human eggs, 10 minutes for pig eggs and 14 minutes for mouse eggs. Following the cold-treatment, the dish was removed from ice and the cells were immediately fixed and processed for immunofluorescence microscopy. K-fiber attachments were quantified from three-dimensional volume reconstructions of spindles using Imaris (Bitplane) or maximum intensity projections of selected z sections using Fiji (SciJava).

Oocyte immunofluorescence

Before fixation, the oocyte were pre-permeabilized by a brief 10 s exposure to 0.25% Triton X-100. Oocytes were then fixed (30 min for mouse oocytes; 60 min for pig or human oocytes) at 37°C in 100 mM HEPES (pH 7; titrated with KOH), 50 mM EGTA (pH 7; titrated with KOH), 2% formaldehyde (methanol free) and 0.2% Triton X-100. Afterward, oocytes were extracted overnight at 4°C in PBS supplemented with 0.1% Triton X-100. All antibody incubations were performed in PBS, 3% BSA and 0.1% Triton X-100, either overnight at 4°C (primary antibodies) or for 3h at room temperature (secondary antibodies). Primary antibodies used were human ACA centromere CREST autoantibody (FZ90C-CS1058, Europa Bioproducts; 1:500 and 15-234-0001, Antibodies Incorporated; 1:50), rabbit anti-CENP-F (ab5, Abcam; 1:100), sheep anti-BubR1 (Abcam, ab28192; 1:50), mouse anti-Hec1 (ab3613, Abcam; 1:100) and rat anti-α-tubulin (MCA78G, Serotec; 1:1000). As secondary antibodies, Alexa Fluor488/564/647 labeled anti-mouse/anti-rabbit/anti-human/anti-sheep/anti-rat (Thermo Fisher; 1:400) were used. DNA was stained with 5 mg/ml Hoechst 33342 (Molecular Probes).

Immunofluorescence of tissue culture cells

NIH 3T3 and HEK293T cells were seeded in 35mm glass-bottom imaging dishes (MatTEK). Cells were then pre-permeabilized with 0.25% of Triton X-100 for 60 s and fixed for 10 min in 100 mM HEPES (pH 7; titrated with KOH), 50 mM EGTA (pH 7; titrated with KOH), 2% formaldehyde (methanol free) and 0.2% Triton X-100. Primary antibody was diluted in PBS, 3% BSA and 0.1% Triton X-100 and the cells were incubated for 1.5h at room temperature (ACA centromere CREST autoantibody, FZ90C-CS1058, Europa Bioproducts; 1:500). Alexa Fluor488 anti-human (Thermo Fisher; 1:500) was used as a secondary antibody and DNA was counterstained with 5 mg/ml Hoechst 33342 (Molecular Probes).

Super-resolution immunofluorescence microscopy

Super-resolution images were acquired using the AiryScan module on Zeiss LSM800 and LSM880 microscopes equipped with 40x C-Apochromat 1.2 NA water-immersion objectives and processed post-acquisition using ZEN2. Images were acquired at a spatial resolution of 0.19 μm optical sections, covering the entire spindle. In experiments used for quantitative assessment of the fragmentation status of kinetochores, the spindles were manually rotated once the imaging dish was placed on the microscope, so that the long axis of the spindle was in parallel to the plane of the imaging dish. To achieve this, a single oocyte at a time was placed in the imaging dish and prior to image acquisition the oocyte was manually rotated with a tip of an unbroken microinjection needle until the desired orientation of the spindle was achieved. Because the resolution in the z-direction is inferior to that in the xy plane in the imaging techniques that we have used, rotating the oocytes to achieve a comparable orientation of the spindle relative to the imaging plane allowed us to make reliable assessments of kinetochore morphologies across different oocytes. Images depicted in the figure

panels were recorded within the dynamic, non-saturated intensity range. The image intensities were then adjusted post-acquisition in a linear way to improve clarity of the displayed structures.

Structured illumination microscopy (SIM) of human eggs was performed on a Zeiss ELYRA S1 (SR-SIM) system equipped with a 63x C-Apochromat 1.2 NA water-immersion objective. Images were acquired at an optical slice thickness of 0.12 μm confocal sections, covering ∼20 μm.

Stimulated emission depletion microscopy (STED) was performed on a two-color Abberior STED 775 QUAD scanning microscope (Abberior Instruments GmbH) equipped with 488 nm, 561 nm, and 640 nm pulsed excitation lasers, a pulsed 775 nm STED laser and a 100x oil immersion objective lens (N.A. 1.4). Pixel size was 20 nm for all of the images. Laser powers and dwell times were kept constant between samples.

Confocal microscopy in fixed cells

To establish the effect of Trim-Away on the centromeric cohesin pool, we imaged chromosome spreads of metaphase-II mouse eggs using confocal microscopy. Trim-Away experiments in MII eggs were performed as described above. To compare the fluorescence of the centromeric pool of cohesin complexes between Trim-Away expressing MII eggs microinjected with either a control or an anti-cohesin antibody, both groups across all experimental repetition were imaged on the same microscope (Zeiss LSM880 equipped with a Plan-Apochromat 63x/1.4 Oil immersion objective for the anti-Rec8 experiments and Zeiss LSM800 equipped with a Plan-Apochromat 63x/1.4 Oil immersion objective for the anti-Smc3 experiments) using identical imaging settings. The z-intervals used were 0.45 μm and 0.36 μm, respectively, and the same number of z sections covering the entire chromosomal signal was used for the control and the experimental groups.

Confocal microscopy in live cells expressing fluorescent reporters or incubated with fluorescent dyes

Confocal images of live oocytes were acquired using Zeiss LSM800 and LSM880 microscopes at 37.5°C. Oocytes were imaged in M2 medium under oil using a 40x C-Apochromat 1.2 NA water-immersion objective. For chromosome behavior analysis following cohesin depletion the oocytes were typically imaged at a temporal resolution of 4-10 minutes and optical slice thickness of 1.5 μm, covering the entire spindle. To assess spindle dynamics following drug treatments the oocytes were imaged for 7 hours at a temporal resolution of every 15-20 minutes and optical slice thickness of 2.5 μm. Prior to any experiment aiming to perturb kinetochore organization, the general oocyte health was assessed using fluorescently labeled chromosomes and microtubules in live oocytes.

In order to compare the timing of progression through meiosis between oocytes from old and young mice, fluorescent dyes compatible with live imaging were used to follow chromosome (SiR-tubulin, Spirochrome, 1: 10,000) and microtubule (DNA 5-TMR-Hoechst, gift from G. Lukinavičius, 1: 10,000) dynamics. In brief, isolated oocytes were transferred into M2 medium supplemented with dbcAMP and the above-mentioned dyes for 2h hours. To promote release from meiotic arrest, oocytes were washed through droplets of M2 medium lacking dbcAMP and transferred into imaging dishes containing M2 medium and the dyes only. For each experimental repetition, both old and young oocytes were imaged in the same imaging dish placed on the microscope for 22 hours (Zeiss LSM800 or LSM880). Images were acquired every 15 minutes at an optical slice thickness of 2 μm confocal sections covering 66 μm.

Immunoblotting

Oocytes were injected with mRNA coding for TRIM21 and fluorescently labeled chromosome and microtubule markers. Once the oocytes have reached the metaphase-II stage the following day, they were microinjected with anti-cohesin antibody or corresponding IgG control. After 2 hours, the chromosome morphology of each egg was scored by assessing the fluorescence signal on the microscope. Only eggs with roughly half of the chromosomes disintegrated into single chromatids at the time of assessment were selected for the "partial depletion of Smc3" group. The selected eggs were then washed in PBS, transferred in minimal volume of PBS into Eppendorf tubes and snap frozen in liquid nitrogen (20 oocytes per group). On the day of Western Blotting, the eggs were thawed and resuspended in NuPAGE LDS Sample Buffer (Thermo Fisher). The mix was then heated at 95°C for 5 mins. Samples were run at 4°C on NuPAGE 4%–12% Bis-Tris gels (Thermo Fisher) and transferred onto nitrocellulose membrane. Antibody incubations were performed in TBS with 5% skim milk powder (w/v) and 0.05% Tween-20. Primary antibodies used were rabbit anti-Smc3 (Abcam, EPR7984) and anti-α-tubulin (rat, AbD Serotec). HRP-coupled secondary anti-rabbit (Invitrogen, 31462) and anti-rat (Santa Cruz, sc-2032) antibodies were detected by enhanced chemiluminescence (SuperSingal West Femto Maximum Sensitivity Substrate, Thermo Fisher, 34095).

QUANTIFICATION AND STATISTICAL ANALYSIS

Chromosome counting and assessment of kinetochore configuration

All kinetochore fragmentation analysis in chromosome spreads and fixed eggs was performed on images that were acquired using super-resolution microscopy techniques (STED, SIM or AiryScan). Prior to analysis, the AiryScan images were processed post-acquisition using ZEN2.

First, the total chromosome count of an egg was determined by assigning a number to each DNA unit (1-23 in humans, 1-20 in mice and 1-19 in pigs). To achieve this, sister chromatids that form a chromosome were annotated and individual single chromatids were

marked in ImageJ. Subsequently, the kinetochore foci belonging to the same chromosome were identified by comparing CREST/Hec1/CENP-A and Hoechst staining in consecutive z-planes spanning the entire chromosome. The two sister kinetochores of each chromosome were then marked with "A" and "B," corresponding to the appropriate chromosome number.

All detection of kinetochore fragments on chromosome spreads was performed using automated spot detection function based on local maxima in Imaris (Bitplane; expected foci diameter: 200-250 nm). All automated spot detections were confirmed by visual inspection with minimal manual correction. The fragmentation status of a kinetochore was then additionally scored qualitatively by comparing the appearance of each kinetochore in single z sections in ImageJ. In Figure 1J, the "concordant" group includes all kinetochore/centromere pairs, where the automated spot detection function in Imaris detected multiple foci both in the CENPA signal and the Hec1 signal, or both the kinetochore and centromere were compact (single signal focus detected). All surface area, Feret's diameter (the maximum caliper) and circularity (circularity = 4pi x (area/perimeter^2, where circularity value of 1.0 indicates a perfect circle) measurements were performed in ImageJ on maximum intensity projections of appropriate z sections covering the entire kinetochore/centromere region. In Figure 1G, the dispersal of the centromeric domain was measured by comparing the surface area of the smallest circle encompassing the CENP-A signal. In Figure 1A, the fluorescence intensity of the centromere-associated CENP-A pool was quantified per centromere basis by selecting a region of interest (ROI) encompassing that centromere. Subsequently, the integrated density for that region was calculated (computed in ImageJ as Area of the ROI x Mean Grey Value) and finally the mean fluorescence of the background in that region multiplied by the area of the ROI was subtracted. The procedure was then repeated for all the centromeres in a given cell to obtain the egg's total centromeric CENP-A fluorescence. For quantifications in fixed eggs, kinetochore configurations were scored as follows: compact – a single CREST spot visible by inspection of the brightest z-plane, with a uniform single focus in the 3D projection, and fragmented- two or more discrete CREST foci, the outlines of which could be resolved. For fragmented kinetochores, the number of domains that could be resolved with confidence was further annotated. Because in aged mice and in the Trim-Away experiments targeting cohesins in young mice the CENP-A centromeric domain was observed to fragment into numerous foci of a diameter too small for a reliable evaluation of the exact number of foci by automated spot detection, we did not count the number of CENP-A foci and instead measured CENP-A fragmentation by evaluating Feret's diameter, surface area of the domain or its circularity.

Assessment of the effects of Trim-Away mediated cohesin loss on chromosome architecture in the metaphase of meiosis I

The separation between sister kinetochores within the same pair (also known as iKT, intrakinetochore distance) and the distance between the two sister kinetochore pairs (bivalent's long axis or interkinetochore distance) was determined by an assessment of 3D reconstructions of meiosis I spindles fixed at the metaphase stage (Imaris, Bitplane). iKT depends on the amount of centromeric cohesion, while bivalent's long axis is a readout of the physical linkage between the homologous chromosomes of a bivalent and depends on arm cohesion. CREST and Hoechst signals were used to identify the four kinetochores of any given bivalent. The center of each kinetochore was detected with subpixel accuracy using the automated spot detection function based on local maxima in Imaris (Bitplane). The iKT and bivalent long axis length were then computed in Microsoft Excel using the Pythagorean Theorem on xyz coordinates of kinetochore centers defined by the automated spot detection function. In instances were the two sister kinetochores were too tightly linked to be resolved as two independent spots by AiryScan microscopy, the iKT was set to 0 μm.

Modes of kinetochore-microtubule attachment

All eggs that were included in the analysis were recorded using super-resolution microscopy techniques and single eggs were rotated on the microscope prior to image acquisition, as described in detail in the microscopy section above. Microtubule-kinetochore attachments were determined by 3D analysis of appropriate z sections. For quantification of k-fibers involved in an interaction, first the number of discrete k-fibers attaching to a kinetochore was determined. Then, the fragmentation status of the kinetochore was linked to its attachment mode, based on number assigned to the chromosome/chromatid (as described above). For k-fiber attachment modes, only kinetochores with end-on attachments originating from opposite spindle poles were included in the merotelic group, whereas k-fibers which were in a direct contact with a kinetochore, but were extending beyond the kinetochore, were scored as lateral.

Quantification of fluorescence intensity of the centromeric cohesin pool

The quantification of the efficiency of Trim-Away mediated depletion of the centromeric Rec8 and Smc3 cohesin pools was performed on MII chromosome spreads imaged with Zeiss confocal microscopes, as described above. All repetitions for each of the two experiments were performed on the same microscope using identical imaging conditions. The number of z sections recorded was the same for the control and the experimental group. Subsequently, a Sum Intensity Projection of all z sections was performed and the signal intensities were compared in ImageJ. In brief, first the centromeric region in each chromosome was identified in the control group using the CREST channel and an ROI (Region of Interest) was marked using a free drawing tool. Thus, the ROI included the two sister kinetochores of a chromosome and the centromeric regions located medially to the kinetochores. The ROI was then copied to the Rec8/Smc3 channel by using the ctrl+shift+E command and the Mean Intensity of the Rec8 signal in that region was computed. This procedure was performed for all remaining chromosomes in any given cell, with the area of ROI being kept constant. In our experimental group, the Trim-Away targeting of Smc3 or Rec8 resulted in the complete separation of chromosomes into sister chromatids, which was in line with our prediction. Analogous to the control cells, a ROI encompassing a kinetochore and its

centromere was selected for each chromatid. The area ROI was kept constant for all measurements and as predicted from the separation of all chromosomes into single chromatids in our assays, the area occupied by the kinetochore and its centromere in the Trim-Away experimental group was roughly half of that in control cells, in which the two sister chromatids were still linked. To determine the value for background in our images, we calculated in each control/experimental cell the mean background intensity across five randomly selected regions on distal chromosome arms, which in meiosis II are cohesin-free. Subsequently, we computed the Final Fluorescence Intensity as Mean Fluorescence Intensity of ROI – Mean Background Intensity. In the few instances where the Mean Background Intensity was higher than the measured Mean Fluorescence Intensity in the centromeric region (0.78% for the control measurements, n = 510 and 9.75% for the Trim-Away experimental group, n = 800), likely indicative of centromeric cohesin depletion to a level that is lower than non-specific background signal, the negative values were assigned as zero. The values in each experiment were subsequently normalized to the mean Final Fluorescence Intensity of the control group, and all Final Fluorescence Intensity measurements were plotted in the form of boxplots.

Quantification of western blot mean band intensity

To assess the specificity and efficiency of protein depletion using the Trim-Away approach, the mean band intensities of the Smc3 signal were normalized to the intensity of the loading control standard (α-tubulin signal). Gel analysis plugin in ImageJ was used to quantify the band intensity and mean across three experimental replicates was calculated. All control and experimental groups for each experiment were blotted on the same membrane and exposed uniformly to the ECL solutions.

Statistical analysis

Average (mean), standard error of the mean and standard deviation were calculated in Microsoft Excel or OriginPro (OriginLab). Unless specified otherwise, significance analyses were based on Student's t test (always two-tailed) and were calculated using OriginPro. For comparison of absolute values, significance analysis was performed with the Fisher's Exact test using the XLSTAT add-on to Excel. In instances where the absolute values were coming from multiple experimental repetitions, an extension to Fisher's Exact test was applied (Cochran-Mantel-Haenszel test, CMH). Three to six independent experimental replicates were performed for each experiment, with the following exceptions, where two experimental replicates were quantified: Hec1/CENP-C morphology assessment in MII eggs after full Trim-Away, CREST morphology evaluation in partial depletion of Smc3 in meiosis I and upon DMSO/Monastrol treatments, and Smc3 immunofluorescence intensity following Trim-Away. The data describing these experiments is presented in a form of boxplots, with the exception of Figures 3E, 3K, 5F, and 6H, where the average fragmentation rate across all samples is plotted. For quantitative analysis of these experiments, the average value of all measurements per oocyte (80 kinetochores in meiosis I and 40 kinetochores in meiosis II, in at least 20 oocytes microinjected twice) was compared by one-way ANOVA followed by Turkey's test to compare the experimental groups. In Figure 1A, the Integrated Density of 42 eggs coming from three independent experimental replicates was normalized and compared as above, with the total centromeric CENP-A intensity per egg compared across the two groups. The STED measurements in Figure 1G were performed on 1776 kinetochores from young/aged mice and 46 independent images were acquired. P values are designated as $*p < 0.05$, $**p < 0.01$, $***p < 0.001$ and $****p < 0.0001$. Non-significant values are indicated as "N.S." All diagrams were generated using Origin 8 Pro. All box plots show median (horizontal lines), mean (small squares), 25th and 75th percentiles (boxes), and 5th and 95th percentiles (whiskers).

DATA AND CODE AVAILABILITY

This study did not generate any unique datasets or code.